2001

Simulation of coupled groundwater flow and transport of heat in the groundwater system under Vestre Lovénbreen, with the model METROHEAT

A surveying study

M.J. van der Ploeg

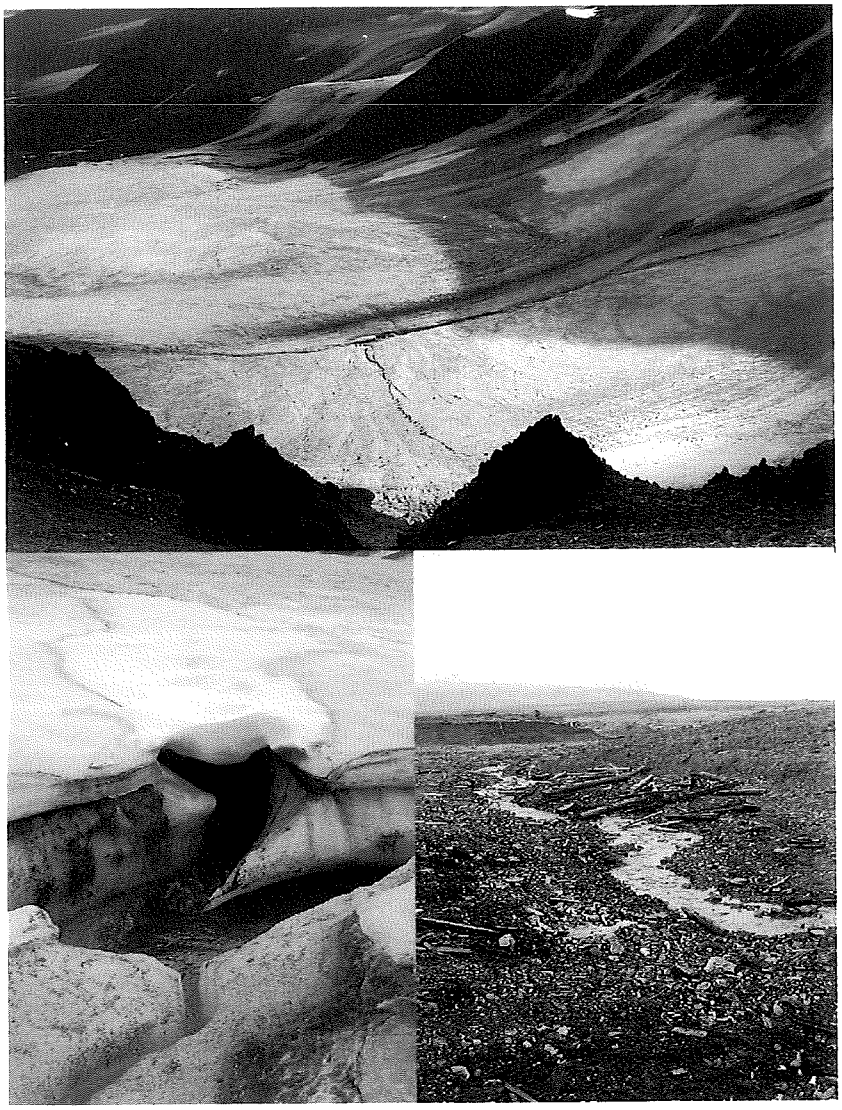

August 2002

WAGENINGEN UNIVERSITY
ENVIRONMENTAL SCIENCES

Simulation of coupled groundwater flow and transport of heat of the groundwater system under Vestre Lovénbreen, with the model METROHEAT
A surveying study

M.J. van der Ploeg

Wageningen, August 2002

WAGENINGEN UNIVERSITY
ENVIRONMENTAL SCIENCES

Preface

Why does a Dutch student want to go to Svalbard to study a groundwater system under a glacier? The mean annual air temperature is well below zero. There are no glaciers in The Netherlands. There is the need to protect oneself against polar bears.
Svalbard is a geological picture book and due to the 'greener garden of the neighbour'-principle, glaciers are attractive. As was the opportunity to study a groundwater system in rock instead of one in sand I always had as an example in my lecture books.

During this research I spent 5 months in Norway at the Agricultural University of Norway and 2 weeks of fieldwork on Svalbard. I did the remaining work at Wageningen University.
Without the help of numerous persons and institutions this thesis would not have been this thesis.

The discussions I had with my supervisors have been very important. I want to thank Sylvi Haldorsen and Michael Heim from the Agricultural University of Norway, who explained me the hydrology and geology of Svalbard, especially about the Ny-Ålesund area. They introduced me to the Norwegian life, for which I am most grateful.
Many thanks go to Toon Leijnse. He answered all my questions about the model METROPOL and adapted the model for me. We had valuable discussions about the model of the groundwater system under Vestre Lovénbreen.
I also want to thank my supervisors for their useful comments on the content and the text of this thesis.

I am most grateful to The Molengraaff Fund for making it financially possible for me to carry out my fieldwork in Ny-Ålesund.
Special thanks go to Morten Røros. We had a pleasant collaboration during the fieldwork on Svalbard and he was so friendly to instruct me how I should handle a polar bear and a rifle. I express my appreciation to Bernard Lefauconnier, who made it possible that Morten and I could stay at the IFRTP (French Institute for Polar Research and Technology). Bernard guided the tour over Vestre Lovénbreen and offered to catch me in case I fell. Morten, Bernard, and I had valuable discussions about the groundwater system, the Vestre Lovénbreen and Ny-Ålesund.

I want to thank Jan Ove Hagen, Stein-Erik Lauritzen, Helen French and Paul Torfs.
Jan Ove Hagen from Oslo University answered my questions about permafrost and Stein-Erik Lauritzen from the University of Bergen shared his thoughts about karstification under Vestre Lovénbreen with me.
Helen French from the Agricultural University of Norway and Paul Torfs from Wageningen University answered a lot of questions I had about modelling.

I also would like to acknowledge the DNMI (Det Norkse Meteorologisk Institutt) and the NILU (Norsk Institutt for Luftforskning). The DNMI provided data of the precipitation and temperature at Ny-Ålesund of the last 25 years. Sverre Solberg of the NILU was so kind to provide me the data of precipitation and temperature of the last 10 years of the Zeppelinstation at Zeppelinfjellet. The State Pollution Authority financially supports the measurements as part of their national monitoring program.

Martine Johanna van der Ploeg
August, 2002

Summary

Svalbard has an arctic climate and glaciers cover about 60% of the land. The almost continuous permafrost layer prevents groundwater recharge in most places on Svalbard. Groundwater recharge takes place under glaciers where the base is at melting point.
The Vestre Lovénbreen is a small glacier near Ny-Ålesund in the northwestern part of Spitsbergen. The low runoff at the front of the glacier indicates a two-part drainage: an upper area where water drains into a moulin and a lower area where water drains to the front of the glacier.
It is assumed that the moulin extends through the whole thickness of the glacier.
The bedrock in the area of the Vestre Lovénbreen consists of Precambrian, Carboniferous, Permian, Triassic and Tertiary rocks.
A spring is situated at the former entrance of an old coalmine close to Ny-Ålesund. The quantity and quality of the water indicate that the water originates from the Vestre Lovénbreen. From the glacier base the water may infiltrate into the underlying limestones, after which it flows through a sandstone aquifer.
In the sandstone the water gets a higher temperature due to geothermal heat.
Mining activities in the past have resulted in the opening of artificial groundwater channels that go through the permafrost zone. From the sandstone the water can flow through the permafrost to the surface. The chemical composition indicates a long storage time in sandstones and a short storage time in limestones.
The spring discharge has decreased due to a decrease in recharge.
To estimate possible consequences for the ecosystem, knowledge of groundwater flow and transport of heat is very important, especially the temperature and velocity distribution, the travel path and the residence time.

METROHEAT is a computer program capable to simulate 3-dimensional groundwater flow and transport of heat in a finite element mesh.
METROHEAT uses averaged forms of the mass and momentum balances of the total liquid phase and the energy mass and momentum balances.
Postprocessing was done with the program Matlab.

A simplified hydrogeological model was constructed for the simulation of the groundwater system under Vestre Lovénbreen. The permafrost layer was incorporated into the model in order to simulate the depth of the permafrost. A 3-dimensional discretisation was made of the area and includes the Vestre Lovénbreen and the groundwater system. The element mesh consisted of deformed cubic elements. With the available data and information a base case and 5 variants for sensitivity analysis were made.
The variants considered the permeability and porosity in the mining area, the spatial variation of the infiltration, the amount of water infiltrating into the system, the interaction between the groundwater flow, temperature and viscosity and the construction of the mesh.

The results of the pressure, temperature and velocity distribution were plotted in surface and contour maps.
The simulated depth of the permafrost layer and the simulated temperature of the outflow point are close to the field data. Estimated residence times of the groundwater in the system are long and very debatable, the estimated residence time in the limestones is 0.6-2 years.
An increase of the permeability and porosity in the mining area did not decrease the residence time of the groundwater. The influence of the spatial variation of the infiltration under Vestre Lovénbreen on the outflow point is small. With a decrease in infiltration of 50% the Ester Spring did not freeze during the simulations, but in the simulations the groundwater system is saturated and in the physical system unsaturated conditions may occur when the infiltration decreases.
The temperature dependence of the viscosity and the deformation of an element mesh should not be underestimated.

Contents

List of figures

List of tables

1 Introduction

Svalbard is a high arctic archipelago, where about 60 % of the land is covered by glaciers (Hjelle, 1993). On large parts of Svalbard groundwater is efficiently prevented by an almost continuous permafrost zone of thickness 150-450 metres (Liestøl, 1980).
The recharge of groundwater is restricted to the temperate basal parts of glaciers (Liestøl, 1977). Discharge from subpermafrost aquifers on Svalbard occurs in the ocean or in well-defined artesian springs (Haldorsen *et al.*, 1999).

The village Ny-Ålesund is situated on Brøggerhalvøya, a peninsula in the northwestern part of Spitsbergen (one of the islands of the archipelago).
Close to Ny-Ålesund, in the area of an old coalmine, a main groundwater spring is situated. The discharge point is at one of the entrances of the former Ester mine. The Ester mine was established in the 1920s, when mining activities created artificial channels through the permafrost. There has been a continuous outflow from the spring since that time (Haldorsen *et al.*, 1999). The regime of the spring and the chemical composition of the water indicate that the water comes from a large aquifer. The amount of water that discharges at the Ester Spring corresponds with a catchment area that has the size of the upper area of the Vestre Lovénbreen (Haldorsen *et al.*, 1996).
Vestre Lovénbreen is the small glacier situated south of Ny- Ålesund. In the upper area of the glacier, the penetration of water from the surface down to the glacier bed is mainly through a well-defined moulin, which extends through the whole thickness of the glacier. From the glacier base the water may infiltrate into the underlying limestones, after which it flows through a sandstone aquifer and the artificial groundwater channels, before it discharges at the Ester Spring. The runoff at the front of the glacier is rather low.

Meteorological records and proxy climatic indicators suggest that air temperatures have risen steadily since industrialisation, particularly in the 20th century (Isaksen, 2001). Arctic glaciers are likely to be sensitive to possible warming through an antropogenic increase in greenhouse gasses (Lefauconnier *et al.*, 1999).
The volume of the Vestre Lovénbreen has decreased since 1920. Also the discharge of Ester Spring has decreased since it was established (Haldorsen *et al.* 1996).
The heat transfer from groundwater, dependent upon water temperatures and water fluxes, controls whether the spring will remain open or not. It is hypothesized that a lower discharge will reduce energy transfer and may results in freezing of the groundwater where the outflow channel passes through the permafrost (Haldorsen *et al.*, 1999).

Discharge of water by springs, like the Ester Spring, plays an important role in the balance of the fragile ecological system on Svalbard. Open groundwater springs form important ecological niches and are a potential water supply source for a modern arctic settlement.
A decreased groundwater discharge may cause changes in the water budgets of lakes and springs and thereby change the conditions for animals and plants, which are dependent upon open fresh water for living conditions and food supply during the winter (Haldorsen *et al.*, 1999). Climatic changes may have serious effects on the fresh water supply.

To evaluate possible changes in fresh water availability, knowledge of coupled groundwater flow and heat transport in the groundwater system is of inestimable importance.
This study focuses on the groundwater system under Vestre Lovénbreen, because it has been the subject of preliminary studies (Booij, 1997; Booij *et al.*, 1998, Haldorsen *et al.*, 1993; Haldorsen *et al.*, 1996; Haldorsen *et al.*, 1999). The geology of the area is rather well described (Orvin, 1934; Challinor, 1967; Bergh *et al.*, 2000).

Coupled groundwater flow and transport of heat in the groundwater system under Vestre Lovénbreen was simulated with the use of the package METROPOL (Sauter *et al.*, 1993). METROPOL contains the program METROHEAT, a 3-dimensional model for simulation of coupled groundwater flow and transport of heat.
The most important objects during the study were the temperature distribution in the system, the travel path and the residence time of the groundwater. The permafrost was incorporated into the model in order to simulate the thickness of the permafrost layer, to see where the simulated lower boundary of the permafrost would occur.
A sensitivity analysis was carried out to investigate the effect of some parameters, assumed important for the groundwater system, the temperature distribution and the groundwater velocities.

A model is a simplification of reality and the real physical system should always be kept in mind. Therefore, fieldwork was carried out in the Ny-Ålesund area. The most important part of the fieldwork was the observation of the Vestre Lovénbreen, the Ester Spring, the geology in the Ny-Ålesund area and the physical boundaries the system could have. Measurements of the discharge, temperature and chemical composition of Ester Spring were carried out.

Chapter 2 will give a general description of Svalbard. After that, the Ny-Ålesund area will be described. A description of the fieldwork is included in this chapter. Chapter 3 describes the package METROPOL, the program METROHEAT and gives the equations for groundwater flow and heat transport METROHEAT solves.
Chapter 4 is a combination of chapter 2 and 3: it shows the construction of the model for the groundwater system under Vestre Lovénbreen. In addition, the different variants used for sensitivity analysis will be described in this chapter.
In Chapter 5 the results will be given, and discussed. Chapter 6 gives the conclusions and recommendations.

2 Description of the area

2.1 Introduction

Svalbard has an arctic climate that differs from temperate areas like The Netherlands. In Svalbard, the thick permafrost and the many glaciers are very important for the groundwater systems. As for all groundwater systems, also the flow is dependent on the bedrock geology and the hydrogeological parameters of the rock, like the permeability and the porosity. These subjects will be described here. An introduction to the geography, geology and groundwater occurrence on Svalbard is given in section 2.2. In section 2.3, a detailed description of geography, geology and groundwater system is given for the Ny-Ålesund area. In this section the fieldwork that was done in Ny-Ålesund is included.

2.2 Svalbard

2.2.1 Geography of Svalbard

Svalbard is the geographical name of a group of islands, situated between latitudes 74^0 N and 81^0 N and longitudes 10^0 E and 35^0 E (Figure 2.1).

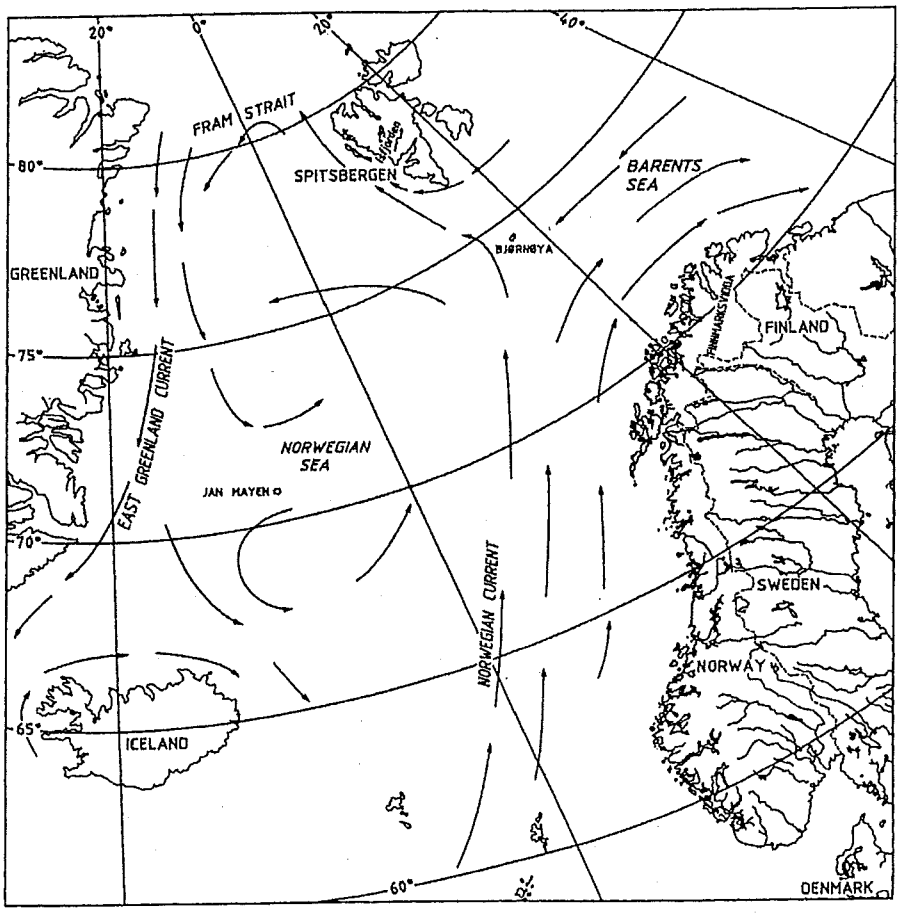

Figure 2.1. Geographical position of Svalbard (modified from Larsen et al., 1991).

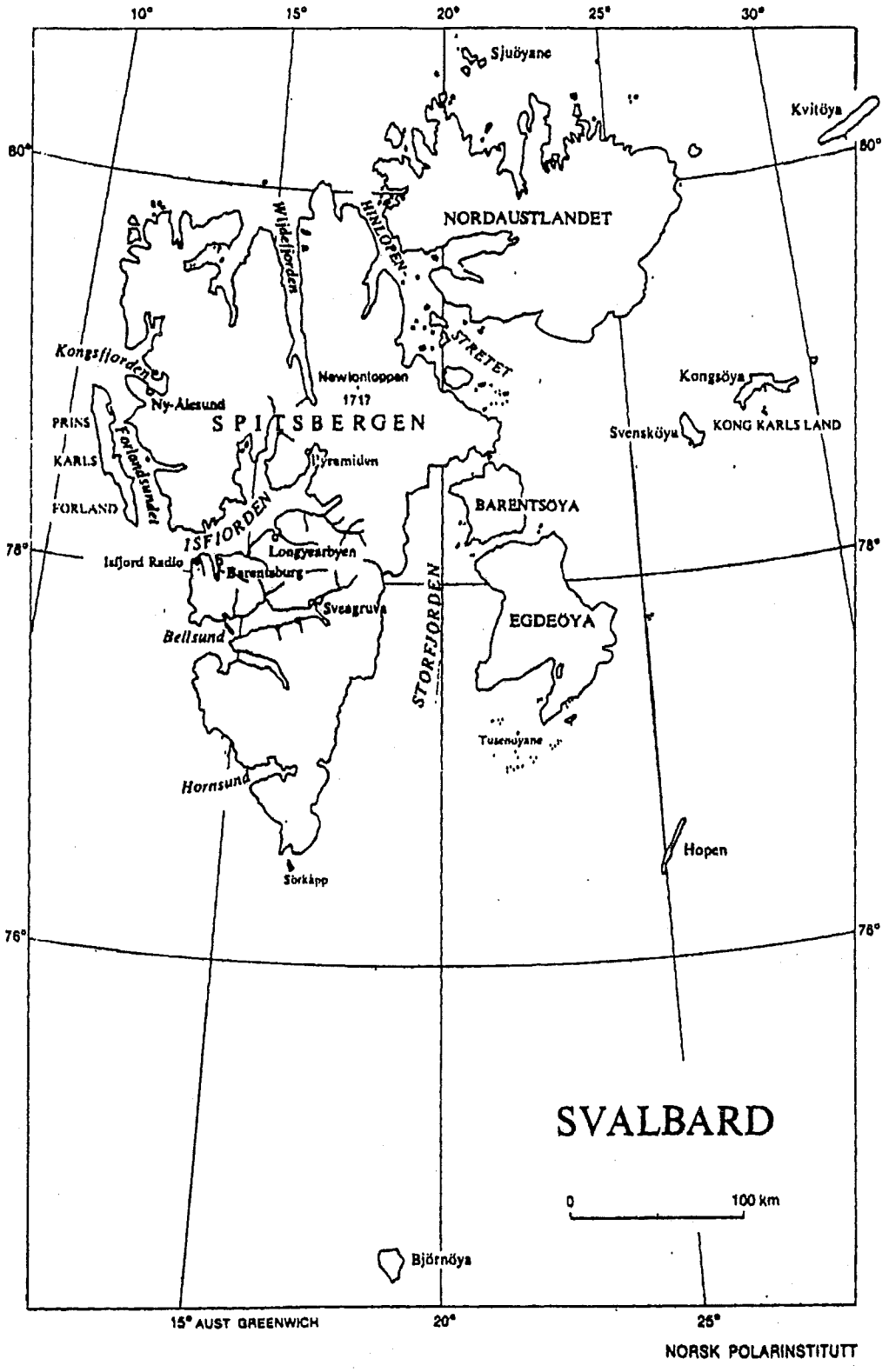

Figure 2.2. Map of the Svalbard Archipelago

Spitsbergen is by far the largest island, followed by Nordaustlandet, Edgeøya, Barentsøya and a whole series of smaller islands (Figure 2.2). The total area of the Svalbard archipelago is about 63,000 km^2 (Hisdal, 1985), which is approximately the size of Belgium and The Netherlands together.

Climate
The climate of Svalbard is considered to be of a Tundra-type, with at least one month with a mean air temperature above 0 ^{0}C. The mean annual air temperature on Spitsbergen varies between –7 °C and –2 °C. The mean annual precipitation at the weather stations on Spitsbergen is 180-400 mm (Hanssen-Bauer *et al.*, 1990).

Glaciers
Glaciers cover about 60% of the land area of Svalbard. These are particularly extensive in the northeast; Austfonna on Nordauslandet being the largest one.
In the west there are almost ice-free areas, due to two factors: the warm waters of the final branch of the Gulf Stream (the North Atlantic Current), which is flowing towards the west coast of Spitsbergen, and mild air currents from the south (Hisdal, 1985).
The glaciers are commonly of a subpolar (multi-thermal) type, with permafrost in the front, and temperate bottom conditions occurring above the glacier equilibrium line altitude (ELA) (Haldorsen *et al*, 1999). The equilibrium line divides the glacier into an accumulation area where during a year more snow accumulates than ablates and an ablation area where the opposite occurs (Paterson, 1981).
The coldest Holocene period in Spitsbergen (the Little Ice Age) lasted for a couple of hundred years and terminated at the end of the 19th century, when glaciers had their largest extent since the Weichselian. Around 1900 the glacier equilibrium line altitude (ELA) was about 200m above sea level, today the ELA is about 200m higher.
By 1920, the climate had changed and become milder, and the glaciers have retreated continuously since that time. As a consequence, more of the basal ice has gradually become cold, and more permafrost is established along the bottom of the glaciers (Haldorsen *et al.*, 1999).

Permafrost
Permafrost is defined as soil or rock having a temperature below 0 °C for a period of at least two years (Van Everdingen, 1997). Permafrost occurs in areas with mean annual air temperatures below –0.5 °C (Van Everdingen, 1997).
On Svalbard the mean annual air temperature is well below zero and the thickness of the permafrost is about 100-400m (Liestøl, 1980). There are large differences between coast and inland (Liestøl, 1977).
Local distribution of permafrost is controlled by factors as exposure, vegetation, extent and duration of snow cover, and by the presence of rivers, lakes and glaciers (Van Everdingen, 1997). Permafrost is absent beneath the temperate parts of glaciers, fjords and large lakes (Liestøl, 1977).

With respect to the relation of permafrost and groundwater, three types of aquifers can be distinguished (Tolstikhin *et al.*, 1976):

1. Suprapermafrost water, which occurs above the permafrost, with permafrost serving as a water impermeable floor.
2. Intrapermafrost water, which is found between layers of permafrost.
3. Subpermafrost water, which occurs below the permafrost. Permafrost acts as an impermeable upper boundary for this type of aquifer.

2.2.2 Geology of Svalbard

Svalbard has not always had the shape and size it has today. The land areas that can be seen today are elevated parts of the Norwegian continental shelf in the Barents Sea, the Svalbard Platform (Hjelle, 1993).
The geographical location of Svalbard has not been constant either. The Caledonian mountain chain was formed about 400 million years ago when an easterly continental plate collided with a westerly one. Since then, the part of the European Plate on which Svalbard lies has mostly drifted northwards, through tropical and desert regions, to the arctic (Hjelle, 1993).
Some major horizontal movements took place at the end of the Devonian period when the Variscan orogeny started and the supercontinent Pangea developed. After a quiet period in the Early and Middle Mesozoicum, Laurasia (northern part of Pangea) fragmented and the Atlantic Ocean developed. During the transition between the Cretaceous and the Tertiary segments of the European plate began drifting independently from each other. First Norway drifted away from Greenland, forming the Norwegian Sea. In the north, compression and thrusting took place, resulting in the belt of Tertiary folding and faulting now seen on the west side of Spitsbergen. Later around Mid-Tertiary time, a period of north-south drifting was initiated and Svalbard began drifting away from Greenland, forming the Greenland Sea (Booij, 1997). A geological timetable can be found in annex A and a geological map of Svalbard in annex B.

Precambrian to Lower Silurian
The oldest formations are found as a belt along the west coast of Spitsbergen (Hisdal, 1985). Rocks of Precambrian to Lower Silurian age are called the Hecla Hoek series or Pre-Old Red (Hjelle, 1993; Dallmann *et al.*, 1999). They are being dealt together, because in Svalbard they compromise more or less metamorphosed and folded rocks.
Several periods of folding and metamorphism have affected all Hecla Hoek series.
Because of the weathering and erosion, only the eroded remnants of the ancient, folded and metamorphosed basement can be seen today (Hjelle, 1993).

Silurian and Devonian
Two continental plates, the Canadian-Greenland plate (Laurentia) and the Fennoscandian Plate, collided at this time, causing large scale folding and faulting (the Caledonian Orogeny). Northern Spitsbergen began sinking and eroded material from the Hecla Hoek basement accumulated in fresh or brackish water (Hjelle *et al*, 1982).
Where the Devonian beds are absent, either because they were never deposited or because they have been removed by erosion, the Carboniferous rocks lie directly on the basement (Hjelle, 1993).

Carboniferous and Permian
During the first part of the Carboniferous, Svalbard was still a relatively flat land area with lakes, lagoons and alluvial plains and the lowermost Carboniferous beds consist of fluvial or deltaic deposits. However, the Svalbard plate gradually drifted to wetter, more tropical areas, where light gray Lower Carboniferous sandstones were formed.
The sea began flooding over the land in the middle of the Carboniferous and the Upper Carboniferous mostly consists of marine deposits; typical rocks are breccias, limestone and dolomite.
The Lower Permian beds greatly resemble the uppermost Carboniferous.
In the Middle Permian dolomite marine deposits were formed and in the Upper Permian hard, richly fossiliferous flints and green glauconitic sandstones were deposited (Hjelle, 1993).

Triassic, Jurassic and Cretaceous
During the Mesozoic, Svalbard drifted from 45°N to 60°N and the climate was largely temperate and humid. Marine deposits are most widespread. The rocks from this period are mostly shales, siltstones and sandstones.
The land surface had largely been leveled and conditions were more stable than in Carboniferous and Permian times. Faulting was almost confined from Jurassic to Cretaceous (Hjelle, 1993).

Tertiary
At the transition between the Cretaceous and Tertiary plate movements began when portions of the Euro-American continental plate started to move relative to one another. Simultaneous with these plate movements, the land was lifted, erosion increased and a distinct break in the succession developed. The Lower Tertiary beds largely consist of sandstones. Luxuriant vegetation formed the basis for several coal seams in this part of the succession.
During this deposition, Svalbard and Greenland were pressed oblique against each other and Spitsbergen was exposed to pressure from the west. This pressure from the west caused intense folding and thrusting, especially along the west coast of Spitsbergen and sharp, jagged peaks were formed.
In the mid-Tertiary, the plate segments, which until then had been pressed against each other, drifted apart again and there were several episodes of fracturing and faulting.
The crustal movements triggered volcanic activity in northern Spitsbergen towards the end of the Tertiary. Late in Tertiary time, Svalbard had attained more or less its present shape and size, but the sculpturing of the landscape was and is largely carried out during the Quaternary (Hjelle, 1993).

Quaternary
Deposits from the Quaternary are still being formed today. These are mostly unconsolidated deposits formed during and after the last Ice Age. They include moraines, fluvial deposits, littoral deposits, talus and block fields.

2.2.3 Groundwater system in Spitsbergen

The thick and almost continuous permafrost layer prevents groundwater recharge in most places on Svalbard (Figure 2.3). Most of the melt water of glaciers runs to the front of the glacier. In areas where the base of the glacier is at pressure melting point a certain portion of the melting water may flow to the bottom of the glacier and infiltrate along fractures into the underlying bedrock. The general impression has been that this is the main recharge mechanism for subpermafrost groundwater on Svalbard (Haldorsen *et al.*, 1996).
Discharge from subpermafrost aquifers on Svalbard occurs in the ocean or in well-defined artesian springs. Karst springs are common, indicating that karst systems are the most important aquifers in Svalbard, but aquifers in the fracture systems of silicate rocks are also found (Haldorsen *et al.*, 1999).
The springs were probably established at the end of the last glaciation, when the sea level was high due to an isostatic depression of the land. The spring outlets were first submarine, and positioned outside the ice margin. When the land rose and the relative sea level dropped, new permafrost was established. The heat transfer from the upflowing subpermafrost groundwater was sufficient to keep the most prominent groundwater springs open (Haldorsen *et al.*, 1999).
Groundwater temperatures, which may be several degrees centigrade above zero, indicate deep circulation systems where groundwater receives the geothermal heat needed to keep the temperature well above freezing point on its way up through the permafrost.

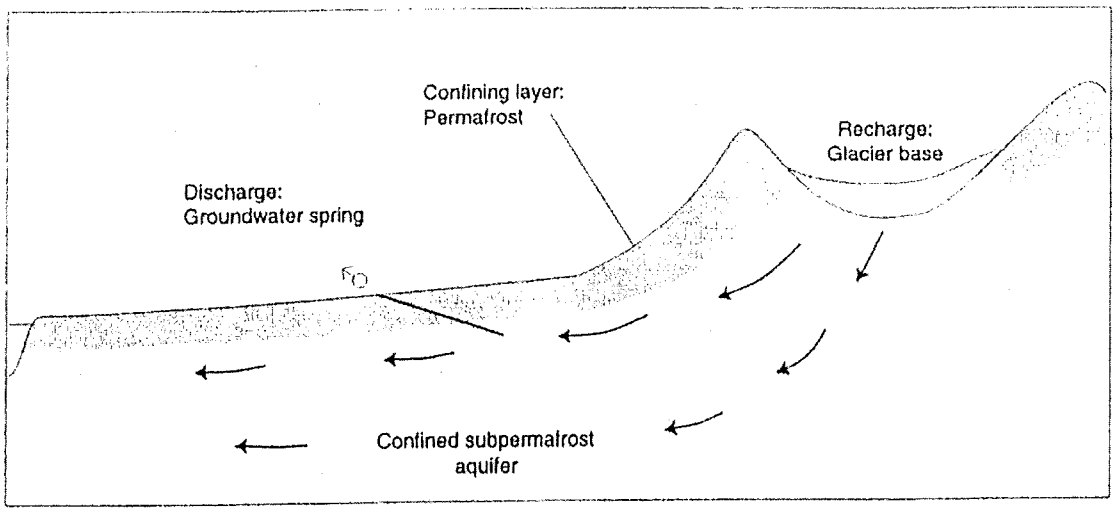

Figure 2.3. Schematical cross-section of a groundwater system (Haldorsen et al., 1996).

Groundwater systems on Svalbard are (in addition to the bedrock properties) controlled by the following time-variable and climate dependent factors:

1. Confining layer	:	The thickness of the permafrost zone.
2. Recharge area	:	The size and properties of the glaciers.
3. Recharge rate	:	The amount of meltwater from the glacier that flows into a groundwater system.

For a short time-scale (50 years), the thickness of the permafrost zone is relatively stable, because it takes a long time to establish equilibrium between the air temperature and the permafrost thickness. Glaciers are quite stable for a relatively short time-scale as well. The recharge rate however, may vary on a short time-scale; the precipitation rate and the air temperature in the summer control the amount of water, which may infiltrate in the ground (Haldorsen *et al.*, 1993).

2.3 The Ny-Ålesund area

2.3.1 Geography

Brøggerhalvøya (Figure 2.4) is a small peninsula on the west coast of the island of west-Spitsbergen.
Ny-Ålesund is situated on the peninsula Brøggerhalvøya, approximately at 79^0 N and 12^0 E, and it is one of the northernmost permanent settlements in the world.
On Brøggerhalvøya 39.5% of the area is below 100 m above sea level (asl), 54% between 100 m and 500 m asl and 6.5% above 500 m asl (Orvin, 1934).

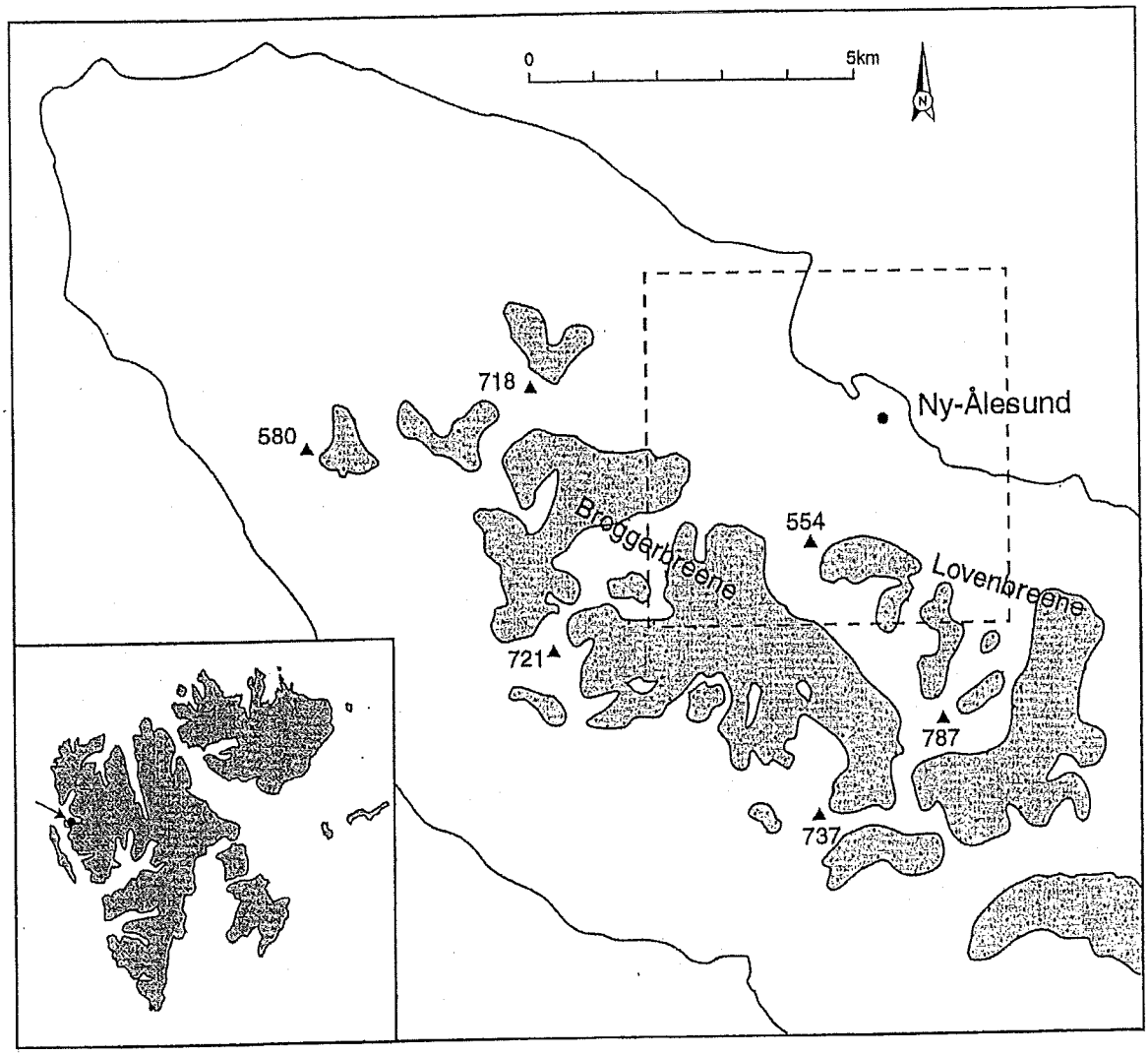

Figure 2.4. Map of Brøggerhalvøya peninsula, dotted square is shown in detail in Figure 2.6. The inset map shows the location of the area on Svalbard (modified from Haldorsen et al., 1999).

Climate
The mean annual air temperature in Ny-Ålesund varied between –8.6 °C and –3.3 °C in the period 1975-2000. The average temperature during the period 1975-2000 was –6.4 °C, measured at an altitude of 8 m asl. The annual precipitation varied between 200 mm and 675 mm with an average of 400 mm during the period 1975-2000 (DNMI Klimaavdelingen, 2001). In Figure 2.5 the average monthly temperature and precipitation for the period 1975-2000 are shown.

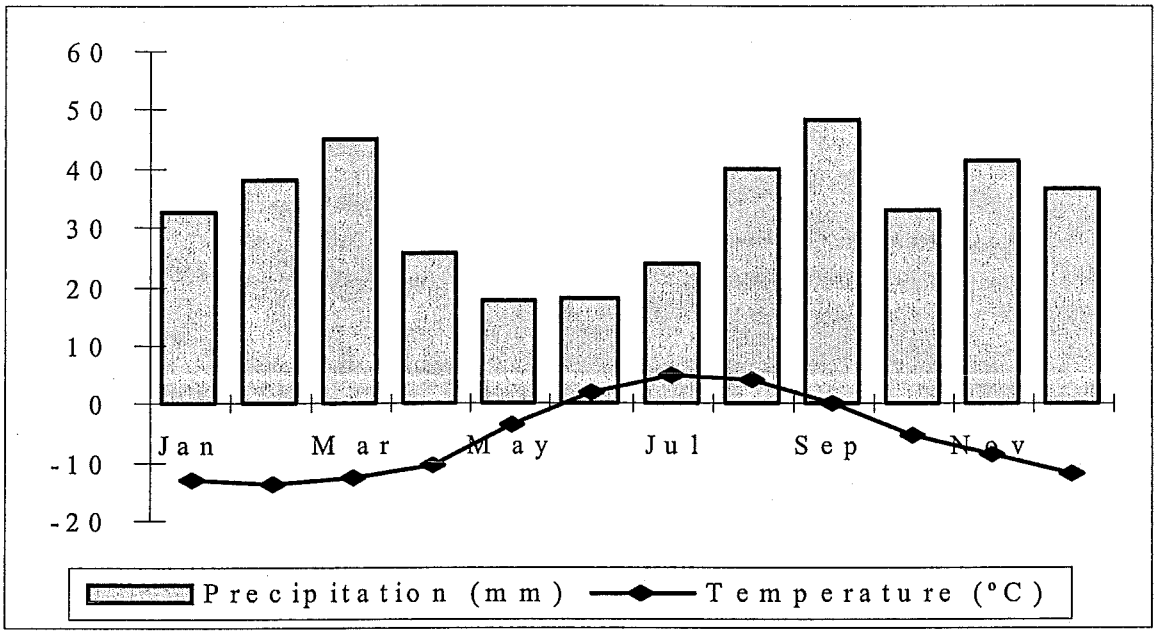

Figure 2.5. Average annual precipitation and temperature in Ny-Ålesund.

Vestre Lovénbreen

The area of Brøggerhalvøya is about 180 km^2 and glaciers cover 25% of it. The rest of the area is covered by marine clay, gravel and river deposits, till, moraine, talus, debris, earth slides due to solifluction. Solid rock exposures can be found on the surface in some places, particularly in the mountainsides (Orvin, 1934).

The glaciers closest to Ny-Ålesund are Austre Brøggerbreen (bre is Norwegian for glacier) and Vestre Lovénbreen (Figure 2.4). The Vestre Lovénbreen (Figure 2.6) is considered to be the groundwater recharge area in this report.

The Vestre Lovénbreen has gradually decreased since the 1920s. From 1920 to 1960 the front retreated, while the upper part of the glacier remained relatively constant. However, during this period the glacier topography of the upper catchment changed from a convex to a slightly concave shape. The area of the glacier is about 2.5 km^2 nowadays. The glacier surface in the area of the moulin was lowered by about 30m during the period from 1921 to 1977 (Haldorsen *et al.*, 1999). The concave form of the whole upper part of the Vestre Lovénbreen indicates that the present glacier has almost no accumulation. The temperate zone along the bottom of the glacier is therefore very limited. With a climate like the present, the whole bottom zone of Vestre Lovénbreen may have temperatures below the pressure melting point within a few decades (Haldorsen *et al.*, 1999).

Permafrost

During the first mining period permafrost in Ny-Ålesund was reported to extend 130-140 m below surface in the mines close to the foot of Zeppelinfjellet and 150 m further out on the plane (Orvin, 1944). During the second mining period, permafrost occurred to be less thick: approximately at 0-50m below sea level (Haldorsen *et al.*, 1996). Liestøl (1977) measured a permafrost depth of 140 m in a borehole next to Tvillingvatn (Tvillingvatn is a small lake in the vicinity of Ny-Ålesund, the location can be seen in Figure 2.7).

Figure 2.6. The Vestre Lovénbreen (photo from Zeppelinfjellet). The location of Zeppelinfjellet can be seen in Figure 2.7.

2.3.2 Bedrock geology of the Ny-Ålesund area

In the following the stratigraphical succession and structure of Brøggerhalvøya and the Ny-Ålesund area will be described. Challinor (1967), Orvin (1934), Hjelle *et al.* (1982), Dallmann (1999) and Bergh *et al.* (2000) give more detailed descriptions. Figures 2.7, 2.8 and 2.9 are illustrations to the text.

Stratigrapical succession
The Precambrian rocks of Brøggerhalvøya consist of highly deformed schists, quartzites, phyllites and dolomites. These rocks form the base of the area and were metamorphosed during the main Caledonian Orogeny. On Brøggerhalvøya these Lower Hecla Hoek metamorphic rocks form the eastern part of the peninsula. They are called the Kongsvegen group (Challinor, 1967).
Rocks of Permian and Carboniferous age have been termed the Gipsdalen Group and consist of the Brøggertinden, Scheteligfjellet, Wordiekammen and Gipshuken Formations.
The Brøggertinden Formation overlies the Hecla Hoek rocks and consists of red and yellow sandstones and conglomerates (Challinor, 1967; Hjelle *et al.*, 1982).
In older literature the Scheteligfjellet and Wordiekammen Formations are called the Nordenskiöldbreen Formation, but the formation is now divided, because of complexity and

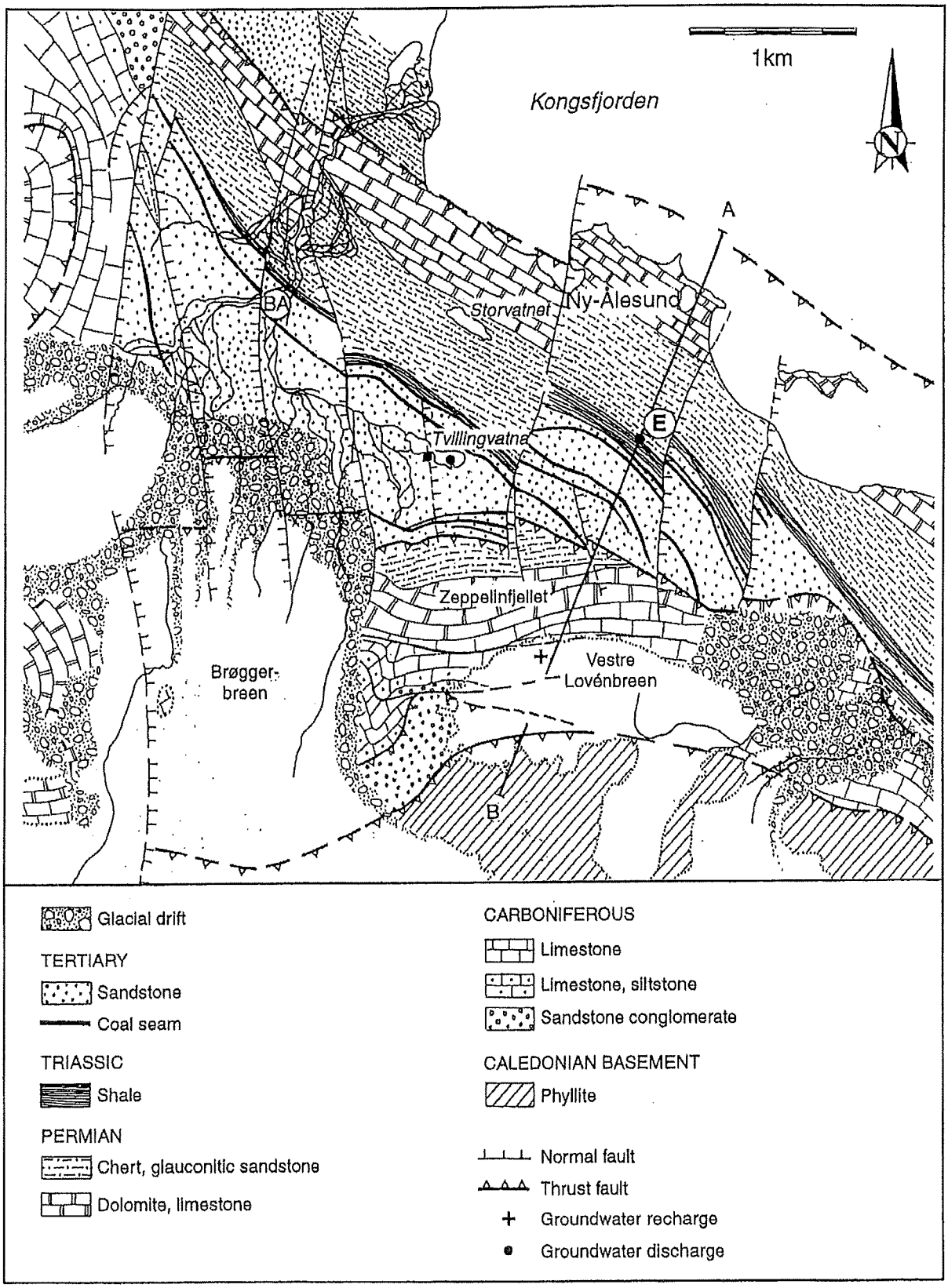

Figure 2.7. Geological map of the Ny-Ålesund area showing the bedrock geology (Haldorsen et al., 1999).

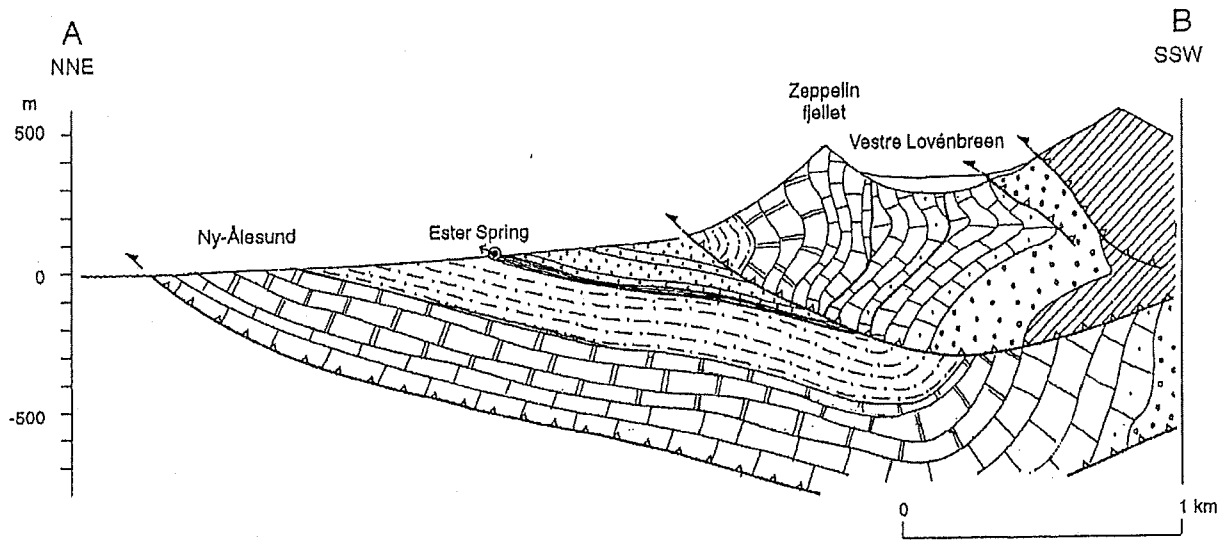

Figure 2.8. Map showing the geological cross-section along A-B in Figure 2.7. Legend: see figure 2.7 (Haldorsen et al., 1999).

heterogeneity (Dallmann, 1999). The Scheteligfjellet Formation marks a transgression and represents a mixed unit of limestone and siltstone.
The Wordiekammen Formation constitutes the upper and main part of the former Nordenskiöldbreen Formation and consists of well-bedded, but heterogeneous limestone and dolomite (Dallmann, 1999;Bergh *et al.*, 2000). The formations were deposited under predominantly shallow marine conditions (Hjelle *et al.*, 1982).
The Gipshuken Formation comprises dolomites with local conglomerates and breccias (Challinor, 1967).
The Kapp-Starostin Formation represents a period of general transgression, producing open marine conduits with the deposition of often fossiliferous beds. The formation is very silicified in parts (Hjelle, 1982; Heim, personal communication, 2001). The formation represents sediments deposited in near shore shallow seas with barrier islands and a distant shelf and consists of cherts, shales and siltstones, glauconitic sandstones (Hjelle *et al.*, 1982).
A thin, fine-grained shale and siltstone unit occurs beneath the Tertiary sequence. Their lithological similarities to the Vardebukta Formation suggest that it is Lower Triassic. The formation represents a shallow-marine, coastal environment (Dallmann, 1999).
The sequence of sandstones, shales, and coal of Tertiary age are termed the Ny-Ålesund Formation (Challinor, 1967).
It contains several coal seams occur, six of them were thick enough to mine. Three of them are situated in the lowermost 20-40 meters of the sequence, namely from below: Ester, Sofie and Advokat seams. About 70 meters above the latter lies the Agnes-Otelie seam and in the upper part of the sequence the Josefine and Ragnhild seams are found (Orvin, 1934).

Structure
The peninsula of Brøggerhalvøya is situated in the region of Svalbard most strongly affected when Greenland was pressed obliquely against Svalbard at the transition between the Cretaceous and Tertiary (Hjelle, 1993).
Tertiary folding and overthrusting have caused northerly movement in Brøggerhalvøya, with Hecla Hoek rocks folded and thrust over the unmetamorphosed Permo-Carboniferous and Tertiary rocks. Accompanying faults appear to be a product of the same stress that produced the folds and thrusts (Challinor, 1967).

The structure is extremely complex in detail, but in general can be related to a single major feature. This consists of an E-W trending major over-thrust complex (Challinor, 1967).
Simultaneous or subsequent extension resulted in the formation of blocks bound by N-S trending normal faults (Haldorsen *et al.*, 1996). The main faults are named from east to west: Østre, Agnes, Josefine, Brøggerdal Valley, Bay River and Schetelig. Many minor faults are found in between the major ones (Orvin, 1934).

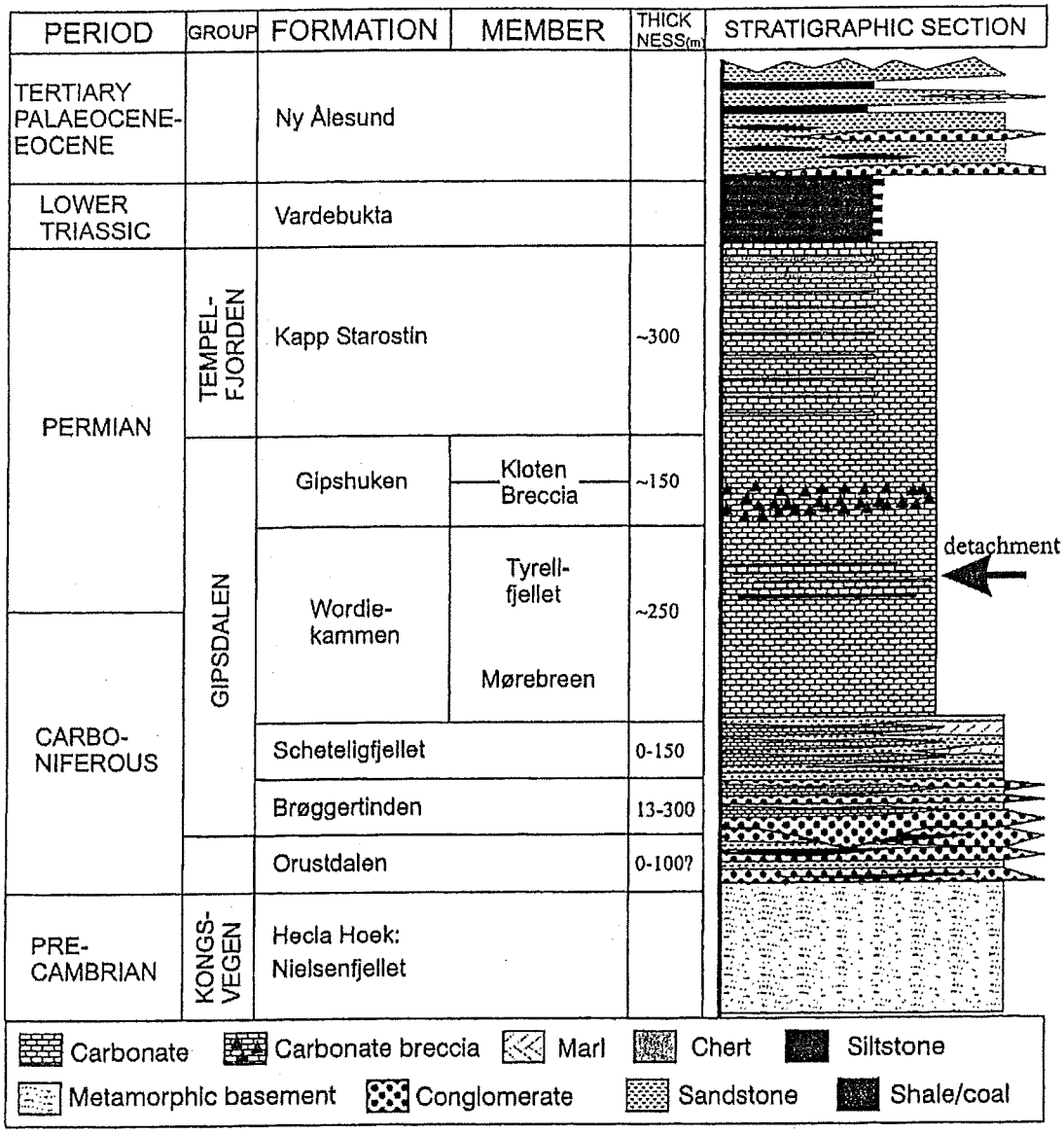

Figure 2.9. Stratigrapical succession of Brøggerhalvøya (Bergh et al., 2000).

2.3.3 Groundwater in the Ny-Ålesund area

Groundwater recharge
The western branch of the Vestre Lovénbreen is of most interest in connection with groundwater. The low runoff at the glacier's front indicates a two-part drainage: the upper area where water drains into a moulin (Figures 2.6, 2.10 and 2.11) and a lower area where the water drains towards

the glacier's front. A subglacial bedrock ridge probably divides the two areas (Haldorsen *et al,* 1999).
The upper catchment (altitude ca. 280 m asl.) with a size of approximately 1km^2 is thus the catchment area for the groundwater.
The moulin is assumed to be a main flow channel for water, which infiltrates into the underlying bedrock (Haldorsen *et al.,* 1996). Several minor steep faults underlie the upper part of the catchment and are believed to be the main groundwater recharge paths today (Haldorsen *et al.*, 1999).

Figure 2.10. Vestre Lovénbreen with the moulin.

Aquifer
The Carboniferous conglomerates, sandstones and limestones and the Permian limestone and dolomite rocks have low primary porosities and permeabilities (See annex C).
The Kapp Starostin Formation has a fraction porosity of 0.12-0.19 and measured permeability values up to $5 \cdot 10^{-11}$ m^2. This sandstone makes up a main bedrock aquifer, and during the coal mine period it was observed that this rock contained significant amounts of pore water (Booij *et al.*, 1998).
The rocks in the Ny-Ålesund area are fractured and faulted and groundwater flows through the main fault systems. It is unknown to what extent the Permian and Carboniferous carbonate rocks in the fault and fracture zones have been dissolved and karstified and form open conduits for the groundwater. Limestones and dolomites directly underlying glaciers are reported to be karstified in other research areas on Svalbard (see e.g. Lauritzen, 1990). It is most likely that the carbonate rocks under Vestre Lovénbreen are karstified as well, and that water flows downwards into the Permian Sandstone through relatively wide and open channels (Booij *et al.*, 1998).
The Vardebukt Formation has a low primary porosity and permeability and does not have open water-conducting fractures. The Tertiary sandstones have low primary porosities and permeabilities and do not form important porous aquifers (Booij *et al.*, 1998).

Figure 2.11. The moulin on Vestre Lovénbreen.

Groundwater flow in the mines

During both coal-mining periods in Ny-Ålesund, groundwater leakage was a large problem in some of the mines. The water flow was considerable whenever one of the main extensional faults was crossed and inflow rates of 15-40 l/s were reported in mines along the Agnes and Josefine faults (Haldorsen *et al.*, 1996). The inflow in mines occurred mainly below the permafrost, where fault zones act as permafrost aquifers.

When the mines were closed after the first mining period in 1929, they were gradually filled by inflowing groundwater. In 1946, when mining started again, there was still an outflow of 3 l/s of groundwater from the Ester mines.

During the second mining period water generally flowed into the mines where the underlying porous Permian sandstone or highly water-conducting faults were penetrated.

The sandstone forms subpermafrost aquifers and the overlying Triassic shale forms a subpermafrost aquiclude.

The mines were situated between the Vestre Lovénbreen glacier and the sea and were almost certainly fed by water from the Vestre Lovénbreen (Haldorsen *et al.*,1999).

Groundwater discharge

After their closing in 1963, the Ester mines became filled with groundwater again. Similar as in 1946, the discharge point of the Ester mines is at one of the former entrances (Figure 2.12).

The present groundwater discharge is 0.012 m^3/s and there is very little or no seasonal variation (Haldorsen *et al.*, 1996, Haldorsen *et al.*, 1999).

No other groundwater discharge points are observed in the Ny-Ålesund area today. The sea-bottom in Kongsfjorden has a thick sequence of fine-grained bottom sediments, which will act as an aquiclude and no major discharge points have been found along the coast. Therefore the Ester spring is the only major discharge point for groundwater in the Ny-Ålesund area today.

Figure 2.12. The Ester Spring.

Groundwater chemistry
The chemical composition of water samples from the Ester mine spring was determined during 1992-1994 (Figure 2.13).
High sodium and silica contents in the groundwater from the Ester mines are due to weathering of silicate minerals. The water is far from equilibrium with calcite and dolomite. This indicates that long residence times in carbonate rocks are unlikely.
The groundwater chemistry thus indicates that the main groundwater aquifers are silicate rocks (chert, sandstones and conglomerates).
The composition of the groundwater is relatively constant during the year with no marked seasonal variations, indicating leakage from a large groundwater aquifer (Haldorsen *et al.*, 1996).
The temperature of the spring water was 0.6 °C (Haldorsen *et al.*, 1996).
Chemical and isotopic analysis of the water from the Ester spring, as well a 2-dimensional computer simulation of the groundwater flow, indicate a groundwater residence time of more than 30 years (Booij *et al.*, 1998, Haldorsen *et al.*, 1999).

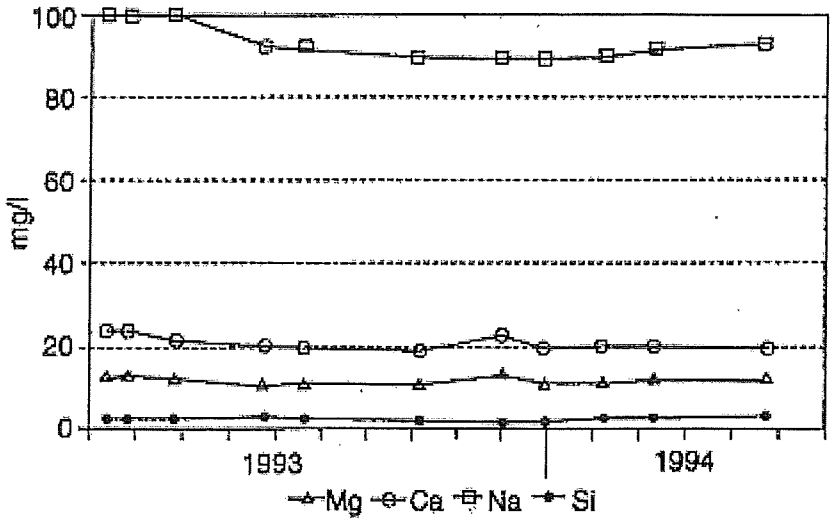

Figure 2.13. Chemical composition of the Ester Spring (Haldorsen et al., 1996).

2.3.4 Fieldwork

Fieldwork was carried out in the Ny-Ålesund area. As stated in chapter 1, the most important part was the observation of the area. This part has been included in the description of the Ny-Ålesund area in sections 2.3.1 to 2.3.3.
Also, some measurements were taken. The results of the measurements will be given here. The methods used to determine the discharge of the spring and the discharge measurements are described in Annex D.

The discharge measured with the salt dilution method was 785.3 l/min. The discharge calculated with the mean section method was 769.5 l/min, with the mid-section method 802.1 l/min.
With the three methods the discharge has a higher value than measured during earlier studies, which was 700 l/min (Haldorsen *et al.*, 1996, Haldorsen *et al.*, 1999). It is not expected that the Ester Spring has a higher discharge nowadays. In the field an inflow of surface water was clearly visible, therefore the measured discharge contained both spring and surface water. It was impossible to determine the quantity of surface water in the measured discharge. It is estimated that the amount of surface water was between 10 and 20%. When the measured discharge would contain about 10% surface water, then the discharge of groundwater would be equal to earlier measurements. When the measured discharge would contain 20% surface water, than the amount of discharging groundwater is less than earlier measurements. New discharge measurements should be done when there is no inflow of surface water, to determine the actual discharge of Ester Spring.
The measured temperature of the water of Ester Spring was 0.9 °C. During the measurement is was made sure that only water of the Ester Spring was measured. The measured temperature is somewhat higher than the temperature of 0.6 °C mentioned in earlier studies (Haldorsen *et al.*, 1996, Haldorsen *et al.*, 1999).

Water samples were taken at the Ester Spring. Precautions prevented that surface water was sampled. The analysis of the water samples was performed by the laboratory of the Soil and Water Department of the Agricultural University of Norway in Ås. The results of the water samples are given in table 2.1.

Table 2.1. Analysis results of the water samples from Ester Spring.

Sample	*Ca(mg/l)*	*Mg(mg/l)*	*Na(mg/l)*	*K(mg/l)*	*Si(mg/l)*	*EC(µS/cm)*	*pH*	*Alk(meq/l)*
1	17.30	15.00	91.5	3.2	2.44	599.0	8.10	4.199
2	16.40	14.80	91.2	3.2	2.32	581.0	8.17	4.163

When the results of the analysis for calcium, magnesium, natron and silica are compared to the measurements in 1992 and 1993 (Figure 2.13), the amounts are nearly the same.
This supported the idea that the chemistry of Ester Spring is very constant, has relatively high amounts of silica and natron and relatively low amounts of magenesium and and calcium and that groundwater discharges from a large aquifer.

At Vestre Lovénbreen, some mass balance measurements have been taken by Lefauconnier (personal communication). The results of these measurements are given in table 2.2. The data are indicative for the situation of Vestre Lovénbreen; the mass balance was negative in September 2001, this means that the volume of the glacier has decreased from September 2000-September 2001.
This can also be seen in figure 2.6, the ice is visible on Vestre Lovénbreen, only on the right of the photo some white areas can be seen, this is snow.

Table 2.2. Mass balance data of Vestre Lovénbreen (Lefauconnier, personal comment).

Stake	*Altitude map (m asl)*	*Altitude winter (m asl)*	*Altitude summer (m asl)*	*Balance winter, cm water equivalent*	*Balance summer, cm water equivalent*	*Balance annual, cm water equivalent*
B7	285	277	*	60	*	*
B8	322	315	314	69(±6)	-72(±3)	-3(±8)
B9	370	380	380	71	-113(±13)	-45

*No data available

3 METROPOL

3.1 Introduction

Groundwater flow and transport of heat in a three-dimensional domain can be described by a system of partial differential equations, supplemented by equations of state, initial and boundary conditions. The partial differential equations follow from averaged forms of the mass and momentum balance of the total liquid phase and the energy balance. The mass balance equations are coupled. Additional equations relate the relevant fluid and rock properties to the primary variables pressure and temperature.
The equations and the coupling between the mass balance equations are too complex to solve analytically. With the help of a numerical method, it is possible to find an approximate solution of the equations.

3.2 The METROPOL package

METROPOL (**Me**thod for **TR**ansport **O**f **POL**lutants) is a software package developed at the RIVM to simulate three dimensional groundwater flow, transport of solutes and transport of heat (Sauter *et al.*, 1993). METROPOL is based on a finite element method, where the elements are topologically equivalent to a cube. The package consists of several sub-packages, capable of tackling different types of problems.

METROPOL-1 :	simulates steady state groundwater flow with a constant liquid density.
METROPOL -2 :	simulates transient groundwater flow with a pressure dependent liquid density.
METROPOL -3 :	simulates transient groundwater flow and coupled salt transport with varying liquid density and viscosity.
METROHEAT :	METROPOL-3 (heat transport version), simulates transient groundwater flow transport of dissolved salt and transport of heat with varying liquid density and viscosity.
METROPOL -4 :	simulates transient transport of a number of decaying and absorbing species with liquid density and viscosity independent on the concentrations.

Although the METROPOL package is primarily designed for application in safety assessment studies of subsurface radioactive waste disposal sites, it can also be applied in other types of studies.

In this study, METROHEAT was used. METROHEAT is a program for the simulation of coupled groundwater flow, transport of dissolved salt and transport of heat under transient conditions.

In addition to the simulation package, several pre- and postprocessing programmes are available. During this study the following were used:

METROMESH :	generates a three dimensional mesh.
METROREF :	refines a previously constructed mesh.
METROPART :	computes particle trajectories in a steady state velocity field.
METROPLOT :	produces data files that can be use to produce graphical results.
METROREAD :	enables inspection of the unformatted data files generated by the different programs and generates plot

files of time profile graphs.

RDARR : is read by input files of several METROPOL modules to read one dimensional double precision arrays.

A description of the equations METROHEAT solves will be given. This study considers groundwater flow and transport of heat. Therefore, only the equations that deal with groundwater flow and transport of heat are mentioned. For detailed information about METROPOL package the reader is referred to METROPOL, User's guide (Sauter *et al.*,1993).

3.3 METROHEAT

3.3.1 Mass balance equations

The mass balance equation for the total liquid phase and the energy balance equation are given by:

$$\frac{\partial}{\partial t}(n\rho)+\nabla\cdot(\rho q)=\rho_{in}I_{in}-\rho I_{ex} \tag{3-1}$$

$$\frac{\partial}{\partial t}\left[(\rho c)_{eff}T\right]+\nabla\cdot\left(\rho c_f Tq\right)+\nabla\cdot J^H=\rho_{in}c_{f,in}T_{in}I_{in}-\rho c_f TI_{ex} \tag{3-2}$$

With:

n	:	porosity [-]
ρ	:	liquid density [$M\cdot L^{-3}$]
q	:	Darcy velocity [$L\cdot t^{-1}$]
I	:	injection or abstraction rate [t^{-1}]
$(\rho c)_{eff}$	:	$= n\rho c_f + (1-n)\rho_{rock}c_{rock}$, effective heat capacity of porous medium [$E\cdot L^{-3}\cdot T^{-1}$]
c_f	:	specific heat of fluid [$E\cdot M^{-1}\cdot T^{-1}$]
ρ_{rock}	:	rock matrix density [$M\cdot L^{-3}$]
c_{rock}	:	specific heat of rock matrix [$E\cdot M^{-1}\cdot T^{-1}$]
T	:	temperature of porous medium [T]
J^H	:	dispersive heat flux [$E\cdot L^{-2}\cdot t^{-1}$]

Subscript *in* denotes injected fluid and *ex* extracted fluid.

3.3.2 Momentum balance equations

The momentum balance equations follow from the simplified averaged forms of the Navier-Stokes equations for the liquid and energy in the individual pores supplemented with appropriate constitutive assumptions. These equations, relating the specific discharge $\boldsymbol{q}$ and the heat fluxes $\boldsymbol{J^H}$ to the primary variables pressure p and temperature T, are known as Darcy's law and Fourier's law. The extended forms of these laws, as derived by Hassanizadeh (1986), modified to account for non-linear flow and dispersion (Hassanizadeh and Leijnse, 1995) can be given as:

$$\left(1+f_q|q|\right)q=-\frac{k}{\mu}\cdot(\nabla p-\rho g)-T^f\cdot\nabla T \tag{3-3}$$

$$\left(1+f_{J^H}\left|J^H\right|\right)J^H=-H\cdot\nabla T-K^T\cdot(\nabla p-\rho g) \tag{3-4}$$

Where:

$$H = \left(n\lambda_f I + (1-n)\lambda_s I\right) + \rho c_f E \tag{3-5}$$

$$E = \left(\alpha_{l,T} - \alpha_{t,T}\right)\frac{q \cdot q}{|q|} + \alpha_{t,T}|q|I \tag{3-6}$$

With:

f_q	:	factor accounting for non-linear flow [$t \cdot L^{-1}$]
k	:	permeability tensor [L^2]
μ	:	liquid viscosity [$M \cdot L^{-1} \cdot t^{-1}$]
p	:	pressure [$M \cdot L^{-1} \cdot t^{-2}$]
g	:	gravity vector [$L \cdot t^{-2}$]
T^f	:	tensor accounting for temperature driven flow, known as thermal osmosis [$L^2 \cdot T^{-1} \cdot t^{-1}$]
f_{j^H}	:	factor accounting for non-linear heat dispersion [$L^2 \cdot t \cdot E^{-1}$]
H	:	total heat flux tensor [$E \cdot T^{-1} \cdot L^{-1} \cdot t^{-1}$]
K^T	:	tensor accounting for pressure-driven heat dispersion [$E \cdot t \cdot M^{-1}$]
λ_f	:	effective thermal conductivity of fluid [$E \cdot T^{-1} \cdot L^{-1} \cdot t^{-1}$]
I	:	unity tensor [-]
λ_s	:	effective thermal conductivity of rock [$E \cdot T^{-1} \cdot L^{-1} \cdot t^{-1}$]
E	:	heat flux dispersion tensor [$L^2 \cdot t^{-1}$]
$\alpha_{l,T}$	:	longitudinal dispersivity in heat flux [L]
$\alpha_{t,T}$	:	transversal dispersivity in heat flux [L]

T^f is a tensor that accounts for flow under influence of temperature gradients. K^T is a tensor that accounts for heat dispersion under influence of pressure gradients. For these tensors and for the permeability **k** it is assumed that the principal axis coincide with the coordinate axes, i.e. all off-diagonal terms are zero.

3.3.3 Equations of state

The mass and momentum balance equations contain a number of physical parameters which have to be related to the primary values pressure p and temperature T. For one of these parameters, the rock density, it will be assumed that it is independent of p and T. The remaining parameters have to be defined as functions of p and T, or both.

The dependence of the liquid density on p and T is given by:

$$\rho = \rho_0 e^{\beta(p-p_r)-\beta^T(T-T_r)} \tag{3-7}$$

With:

ρ_0	:	liquid density at $p=p_r$ and $\omega=0$ [$M \cdot L^{-3}$]
β	:	liquid compressibility [$L \cdot t^2 \cdot M^{-1}$]
p_r	:	reference pressure [$M \cdot L^{-1} \cdot t^{-2}$]
β^T	:	thermal expansion coefficient of fluid [T^{-1}]
T_r	:	reference temperature [T]

ρ_0, β and p_r are constants in space and time. The thermal expansion coefficient is defined as a function of temperature as follows:

$$\beta^T = 2.115 \cdot 10^{-4} + 1.32 \cdot 10^{-6} \cdot T + 1.09 \cdot 10^{-8} \cdot T^2 \qquad (3\text{-}8)$$

A model for the dependence of the liquid viscosity, which considers temperature effects, is given by:

$$^{10}\log\left[\frac{\mu_w(T)}{\mu_w(20)}\right] = \frac{C(T)}{D(T)}\left[1.2378 - 1.303 \cdot 10^{-3} \cdot C(T) + 3.06 \cdot 10^{-6} \cdot C(T)^2 + 2.55 \cdot 10^{-8} \cdot C(T)^3\right] \qquad (3\text{-}9)$$

With:

$\mu_w(T)$	:	liquid viscosity [$M \cdot L^{-1} \cdot t^{-1}$]
$\mu_w(20)$	:	1002 [$\mu Pa \cdot s$] at T = 20 [°C]
C(T)	:	= 20 – T
D(T)	:	= 96 + T
T	:	temperature [°C]

The porosity of the porous medium is assumed a function of the pressure only:

$$n = 1 - (1 - n_0)^{(-C_{eff}(p - p_r))} \qquad (3\text{-}10)$$

$$C_{eff} = \frac{C_{rock}}{1 - n_0} \qquad (3\text{-}11)$$

With:

n_0	:	reference porosity [-]
C_{eff}	:	effective porous medium compressibility [$L \cdot t^2 \cdot M^{-1}$]
C_{rock}	:	rock compressibility [$L \cdot t^2 \cdot M^{-1}$]

The porous medium compressibility and the reference porosity are allowed to vary in space. The reference pressure p_r has a different value from the one used for the liquid density.

3.3.4 Initial conditions

Transient simulations require the definition of the initial distribution of primary variables. METROHEAT requires an initial pressure distribution p and an initial temperature distribution T. In a mathematical sense, the initial conditions can be described independently of each other. However, due to strong coupling between the mass balances, not every description of the initial conditions is physically admissible.

3.3.5 Boundary conditions

The solution to the governing partial differential equations is subject to prevailing boundary conditions. These boundary conditions are formulated in terms of the primary variables p and T. This can be done by fixing the values on the boundary (Dirichlet boundary condition), by defining the derivative in the direction normal to the boundary (Neumann boundary condition), or some combination of the two above mentioned boundary conditions (Robin boundary condition). Instead of specifying the derivatives normal to the boundary, mass fluxes across the boundary can be specified.
Due to strong coupling between the mass balance equations, coupling between the boundary conditions also exists. Therefore, not all combinations of boundary conditions are physically admissible.
In METROHEAT 11 different types of combinations of boundary conditions can be given, ranging from a no-flow boundary to a prescribed total mass flux across the boundary and a well mixed inflow reservoir for temperature.

Minimum requirement of the boundary conditions are given by the continuity of the mass and heat fluxes across the boundaries:

$$\rho q \cdot N|_{-} = \rho q \cdot N|_{+} \tag{3-12}$$

$$\left(\left(\rho c_f + \frac{\beta^T}{\beta}\right)Tq + J^H\right)\cdot N|_{-} = \left(\left(\rho c_f + \frac{\beta^T}{\beta}\right)Tq + J^H\right)\cdot N|_{+} \tag{3-13}$$

Where a minus sign indicates a position just inside the model domain and a plus sign, a position just outside the domain.

3.4 Numerical solution

3.4.1 Finite element method

METROHEAT is based on a Galerkin finite element formulation of the governing partial differential equations describing the flow of liquid and/or transport of heat in a porous medium. The Galerkin finite element formulation results in two sets of non-linear, coupled equations. The Galerkin process is based on an integration of the differential equations over the flow domain. The flow domain is divided into a mesh of smaller blocks or elements and the integrals over the flow domain are computed by summation of integrals over the elements of the mesh. Integration over the elements is done in an approximate way by using two Gauss points in each coordinate direction.

Gauss point values:

$$\iiint_e f(x)dx \approx \frac{1}{8}\sum_{k=1}^{8} J_k^e f_{G_k^e} \tag{3-14}$$

With:

J_k^e : value of the jacobian in Gauss point k

$f_{G_k^e}$: function of the Gauss point k

The Gauss points are given by the local x, y, z-coordinates $\frac{1}{2} \pm \frac{1}{6}\sqrt{3}$ (Figure 3.1).

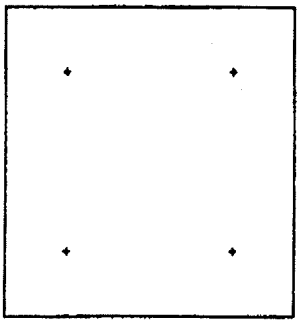

Figure 3.1. Location of the Gauss points in a two-dimensional square element.

3.4.2 Time integration

METROHEAT uses the Euler implicit method for integration in time of the pressure and energy equations and selects the time step automatically. The time step size is restricted by convergence requirements of the non-linear equations.

3.4.3 Mesh

The METROPOL package includes a three-dimensional mesh generator: METROMESH. METROMESH creates a three dimensional mesh of nodal points. The points are the corners of cube-like blocks. The region in which the flow takes place is assumed a three-dimensional domain, topologically equivalent to a cube (Figure 3.2), which means that the cube may be distorted. Each element within the domain has eight corner points.

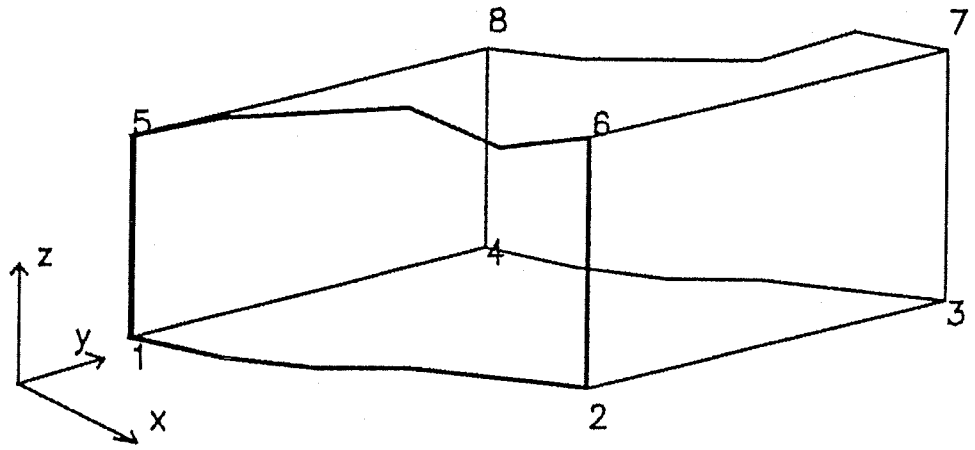

Figure 3.2. Distorted cubic element with corner points.

A restriction in creating the mesh is that the number of nodes in the x-direction must be the same on all YZ-planes. This also holds for the number of nodes in the y- and z-direction. This method combines the advantage of a fixed structure of the nodal points, as in the finite difference method, with some flexibility of the finite element method.
A restriction is needed for the size of the elements in a mesh in order to get a numerically stable algorithm.

In a 1D-transport a sufficient condition for avoiding oscillations is:

$$Pe^m = \frac{\Delta x}{\alpha} \leq 2 \qquad (3\text{-}15)$$

With:

Pe^m	:	mesh Péclet number
Δx	:	block size [L]
α	:	dispersivity [L]

The mesh is constructed by reading coordinates from an input file, or by subdividing edges, surfaces or the internal part of the region into equal parts. During the generation of the mesh, checks are made to ensure that all elements are cube-shaped. When no errors occur, nodal point coordinates are added to an unformatted output file, which can be used as input for METROHEAT.

3.5 Input description

For METROHEAT an input file is required in which the mesh, the parameters for the numerical calculations and data for the hydrogeological properties of the porous medium and the initial and boundary conditions are specified. The data are read from "read array" files (RDARR), which specify the value of a given parameter for all elements/nodal points of the mesh separately or structured in given patterns.
In METROPLOT needs the output files of METROPOL and values for the graphical representation.
METROPART requires an input file in which a mesh and an unformatted output file, values for type of velocity field, stopping criteria and the starting points of the particles are specified.
The input files needed and created by METROHEAT (and for programmes of the METROPOL package in general) are specified with the "USEFIL" (Use Filenames) program (See annex E.1).

3.6 Output

The output of METROHEAT consists of a print file and an unformatted file with pressure distribution, temperature distribution and the velocity in x, y and z direction.
METROPLOT gives output in the form of ASCII files in which the results are listed in rows with x, y, z coordinates and the result value.
METROPART generates unformatted and formatted output, with the coordinate values, travel distances and travel times of the calculated trajectories.
Output files are also specified with the "USEFIL" programme.

4 Construction of a model for the groundwater system under Vestre Lovénbreen

4.1 Introduction

In chapter 2 the geological formations and the groundwater system have been described and chapter 3 handled the numerical model METROHEAT.
In this chapter a description will be given of the simplified hydrogeological model, which was constructed for the simulation of the groundwater system under Vestre Lovénbreen.
The groundwater model needs input data for the initial and boundary conditions and for relevant physical parameters. The input data for the boundary conditions and hydogeological parameters came from the existing field data of the groundwater system. Other necessary physical data were obtained from literature (Booij, 1997; Vågnes *et al.*, 1991; Weast, 1976). In section 4.2 the mesh schematisation and geographical position of the mesh will be described. Physical data are not always available and not every process can be modelled precisely and thus assumptions have to be made; 4.3 describes these assumptions. Section 4.4 describes the hydrogeological and other physical parameters that are needed for the input, section 4.5 the boundary conditions and section 4.6 postprocessing. In annex E.2 an input file for METROHEAT is given.

4.2 Position and schematisation of the mesh

Figure 2.8 in Chapter 2 was used to determine the boundaries of the mesh in xz-direction. Figure 4.1 shows the cross section and the schematised situation in the xz-direction. The area where permafrost occurs was included into the model. The permafrost was not imposed on the model, and the model had to calculate the temperatures in the area of the permafrost. In this way, the results would show the position of the simulated lower boundary of the permafrost. The inflow occurs at the top of the system. Outflow occurs approximately at the Ester Spring.

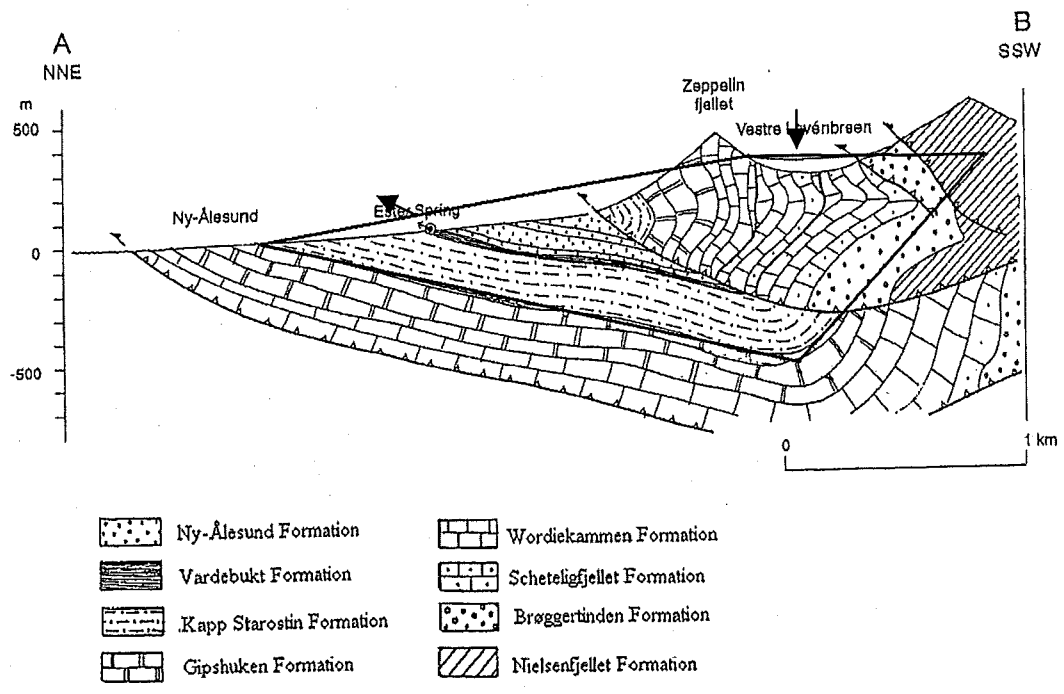

Figure 4.1. Cross section of physical area and schematised area in the xz-direction, the arrows indicate infiltration and discharge (modified from Haldorsen et al., 1999).

The boundary level between the Kapp Starostin Formation and the Gipshuken Formation forms the lower boundary (Figure 4.1). The Gipshuken Formation has a very low primary permeability ($1 \cdot 10^{-16}$-$6 \cdot 10^{-13}$) and porosity (0.001-0.05) and there are no data available for the secondary permeability and porosity. Therefore only the primary permeability and porosity were considered and the Gipshuken Formation was assumed to act as an impermeable base.
The right boundary (Figure 4.1) was arbitrary placed between the Kapp Starostin Formation and the Gipshuken Formation and through the Brøggertinden Formation. The Brøggertinden Formation has a primary permeability of $3 \cdot 10^{-17}$-$6 \cdot 10^{-13}$ m^2, which is very low and water will not flow through this layer, so it acts as a no-flow boundary.
The left boundary does not follow the groundsurface exactly (Figure 4.1), but since this study is a surveying one, this was not considered a problem. The top boundary lies at the level of the glacier and intersects the Brøggertinden and Nielsenfjellet Formation.

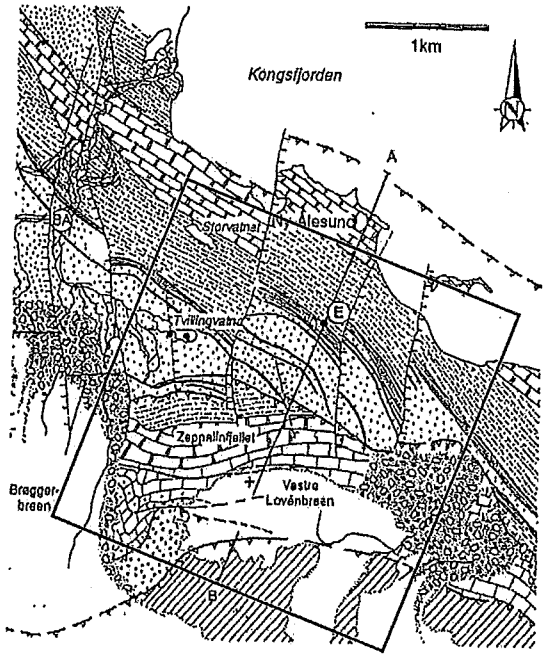

Figure 4.2. The Ny-Ålesund area with the boundary limits in the xy-direction (the boundary is indicated with a square in the figure), legend see figure 4.1.

In the xy-direction the limits were chosen 1500 m parallel on each side of the cross section AB (Figure 4.2). In this way the catchment area of Vestre Lovénbreen and the influence of the groundwater system at the chosen boundaries is assumed to be limited. The limits in xy-direction perpendicular to AB are chosen on the basis of the range in xz-direction.

The finite element mesh was constructed with the program MMESH. This program is described in chapter 3.4.3. The mesh consists of deformed cube-like blocks. The number of nodes in the x-, y- and z-direction are respectively 23, 31 and 18. This gives a total of 12834 nodes. The number of elements in x-, y- and z-direction are respectively 22, 30 and 17, this gives a total of 11220 elements. The averaged size of an element is 72×100×92 m. In annex E.3 an input file for MMESH is given. Figure 4.3 shows the 3D mesh, note that no lines are drawn in the mesh in the z-direction. The mesh is in local coordinates, with a maximum of 2900 m in the x-direction, 3000 m in y-direction and in z-direction the mesh stretches from –500 to 350 m. Figure 4.4 shows a xz-plane of the mesh, in this figure lines are drawn in z-direction as well. Note that the elements are deformed in the x- and z-direction. Figure 4.5 shows a 2-dimensional representation of one of the deformed elements with the angles of the corners.

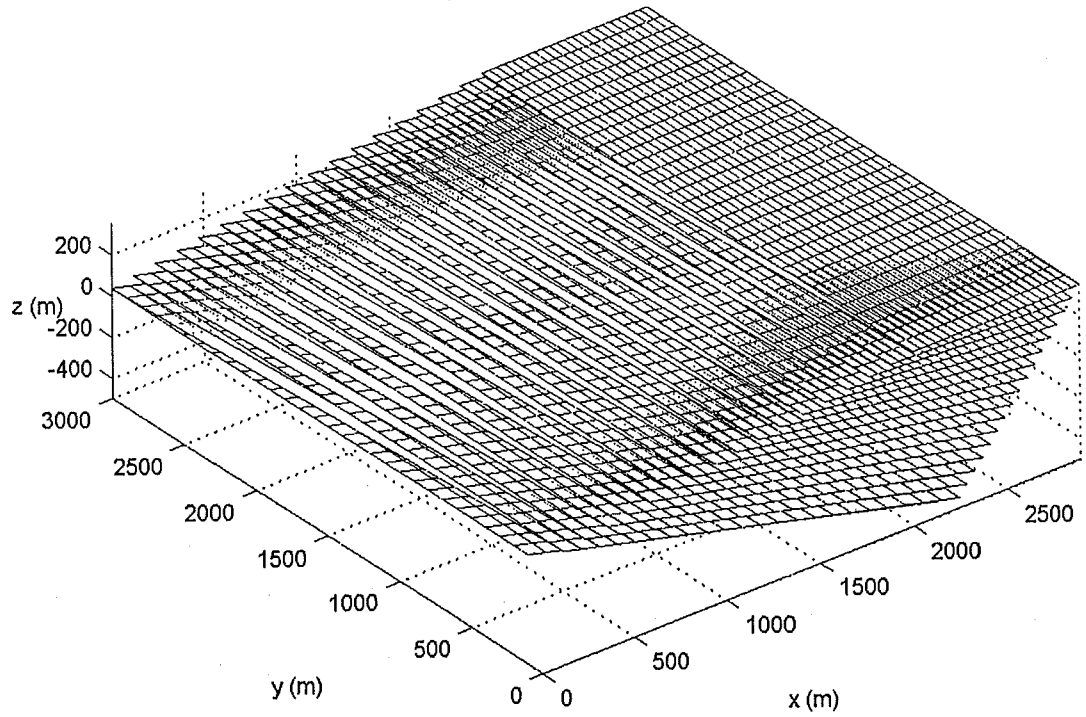

Figure 4.3. The 3D mesh.

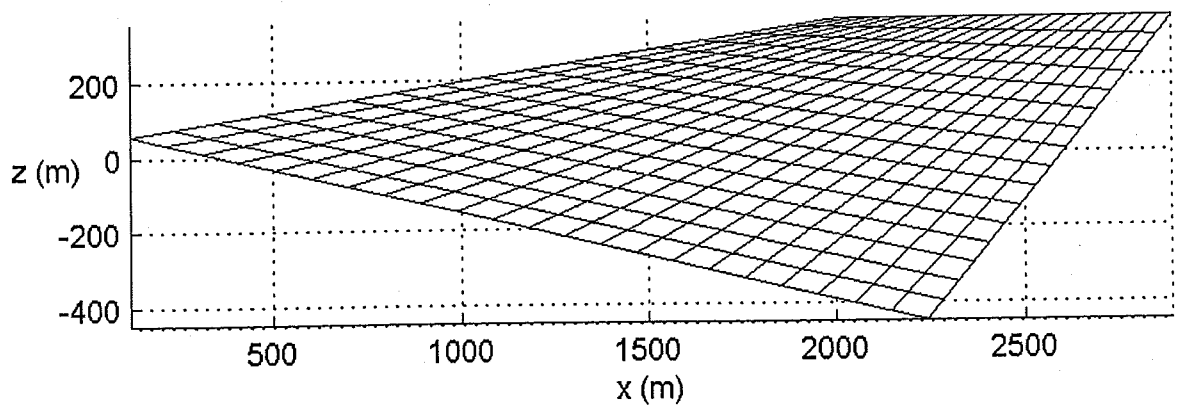

Figure 4.4. Slice of the mesh in the xz-direction.

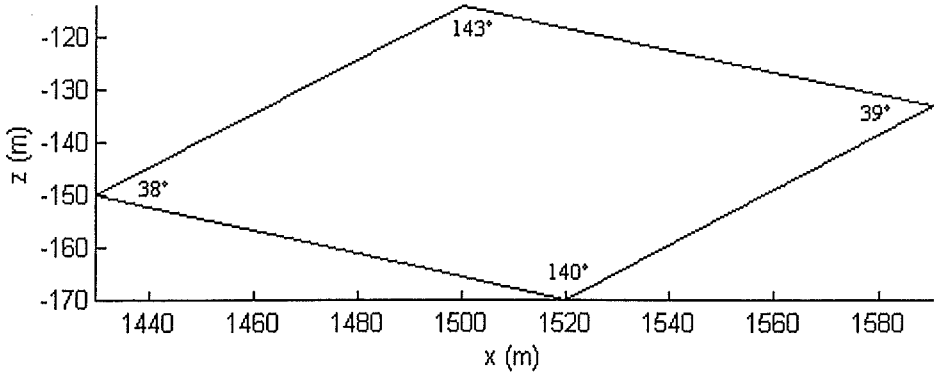

Figure 4.5. A deformed element (2-dimensional representation).

4.3 Simplifying assumptions

During this study it was not possible to consider all effects of groundwater and heat flow through the Vestre Lovénbreen groundwater system, due to lack of data or to limitations of the simulation package. A number of simplifying assumptions was made.

- In the system, the water and the rock are in thermal equilibrium, i.e. the temperature of the solid matrix equals the temperature of the fluid.
- The model solves the groundwater and heat flow equations for temperatures above and below zero.
- Simulation is transient towards a steady-state situation. Some initial conditions are taken arbitrarily and it takes time before a steady-state situation is reached.
- The ground temperature is given by the mean annual air temperature in Ny-Ålesund, the temperature of the top of the system is given by the mean annual air temperature at Zeppelinfjellet, because only data of the air temperature were available.
- Temperature variations in time at the boundaries were not taken into account. The permafrost layer is stable over about 50 years and variations on a short time-scale will not influence the depth. Temperature data for more then 50 years were not available.
- No faults are present in the schematised area. The faults are well permeable and it is assumed that the faults do not have a large influence on the flow. Also, with the METROPOL package it is only possible to model flow through a pore medium.
- Only intergranular flow takes place. METROHEAT only models flow through a pore medium. Further there were no data available about the position and the amount of fractures.
- Density and viscosity are taken constant.
- The porous medium is saturated.
- Compressibility was not taken into account.

4.4 Hydrogeological and other physical parameters

A number of physical parameters are needed as input for METROHEAT. Parameters that are assumed to be independent of spatial position in this study are given in section 4.4.1.
The dispersivities will be described in section 4.4.2 and the spatially varying parameters, permeability and porosity in section 4.4.3.

4.4.1 Constant parameters

A number of parameters independent of spatial position were needed as input for the groundwater model in this study.
The liquid density was set to a constant value (Weast, 1976), because the value of the density does not change significantly within the temperature range that was modelled. It decreases the time (real time) needed for a simulation compared to a situation with temperature dependent densities.
An incompressible fluid has been assumed, therefore the liquid compressibility and the fluid thermal expansion coefficient have been set to zero.
During simulation the liquid viscosity was given a constant value (Weast, 1976). In section 4.6 an explanation will be given for the choice of a constant value for the viscosity.

Table 4.1. The values of different physical properties used during the simulation.

Physical properties	*Symbols*	*Unit*	*Value*
Gravity vector	g	$m \cdot s^{-2}$	9.81
Liquid density	ρ	$kg \cdot m^{-3}$	998.2
Fluid thermal expansion coefficient	β^T	$°C^{-1}$	0.0
Liquid compressibility	β	$m \cdot s^2 \cdot kg^{-1}$	0.0
Reference liquid viscosity	μ	$kg \cdot m^{-1} \cdot s^{-1}$	$1.004 \cdot 10^{-3}$
Fluid thermal conductivity	λ_f	$J \cdot m^{-1} \cdot °C^{-1} \cdot s^{-1}$	0.6
Fluid specific heat	c_f	$J \cdot kg^{-1} \cdot °C^{-1}$	4182.0
Matrix specific heat	c_{rock}	$J \cdot kg^{-1} \cdot °C^{-1}$	840.0
Matrix compressibility	C_{rock}	$m \cdot s^2 \cdot kg^{-1}$	0.0
Matrix density	ρ_{rock}	$kg \cdot m^{-3}$	2650.0
Matrix thermal conductivity	λ_s	$J \cdot m^{-1} \cdot °C^{-1} \cdot s^{-1}$	2.8
Tensor accounting non-linear flow	f_q	$s \cdot m^{-1}$	0.0
Tensor for thermal osmosis	T^f	$m^2 \cdot °C^{-1} \cdot s^{-1}$	0.0
Tensor accounting non-linear heat dispersion	f_{jH}	$m^2 \cdot s \cdot J^{-1}$	0.0
Tensor accounting for pressure-driven heat dispersion	K^T	$J \cdot s \cdot kg^{-1}$	0.0

For the fluid thermal conductivity, the fluid specific heat and the matrix density standard values have been used (Weast, 1976).
Values for the matrix specific heat and the matrix thermal conductivity have been obtained from Booij (1997).
No non-linear flow and heat dispersion, nor osmosis and pressure driven heat dispersion were taken into account, because no information was available about these tensors and they describe second order effects.

4.4.2 Longitudinal and transversal dispersivity

Simulations require values for the longitudinal and transversal dispersivity for heat flux, $\alpha_{l,T}$ and $\alpha_{t,T}$ respectively.
The longitudinal dispersivity is a measure of the size of inhomogeneities in the mean flow direction. The transversal dispersivity is a measure of the size of inhomogeneities perpendicular

on the mean flow direction. The transversal dispersivity is in general one or more orders of magnitude smaller than the longitudinal (Leijnse, 1992). Longitudinal and transversal dispersivity have the dimension length.
No information of the dispersivities in relation with the hydrogeology of the groundwater system was available. In order to get a numerically stable algorithm the longitudinal dispersivity $\alpha_{l,T}$ and the transversal dispersivity $\alpha_{t,T}$ were arbitrarily set to 100 m and 15 m respectively.

4.4.3 Hydrogeological parameters

The spatial distribution of the values for permeability and porosity has been defined with the use of figure 2.8 in chapter 2. The hydrogeological properties for the Nielsenfjellet Formation were taken to equal the ones of the Brøggertinden Formation. The Brøggertinden Formation has a very low permeability and porosity and therefore no water will reach the Nielsenfjellet Formation. Furthermore, there was no information available about the hydrogeological properties of the Nielsenfjellet Formation.
The location of the different formations was implemented in the schematised mesh. In the input of METROPOL the values for permeability and porosity have to be given per element, so the distribution of the different formations is given per element (See figure 4.6).

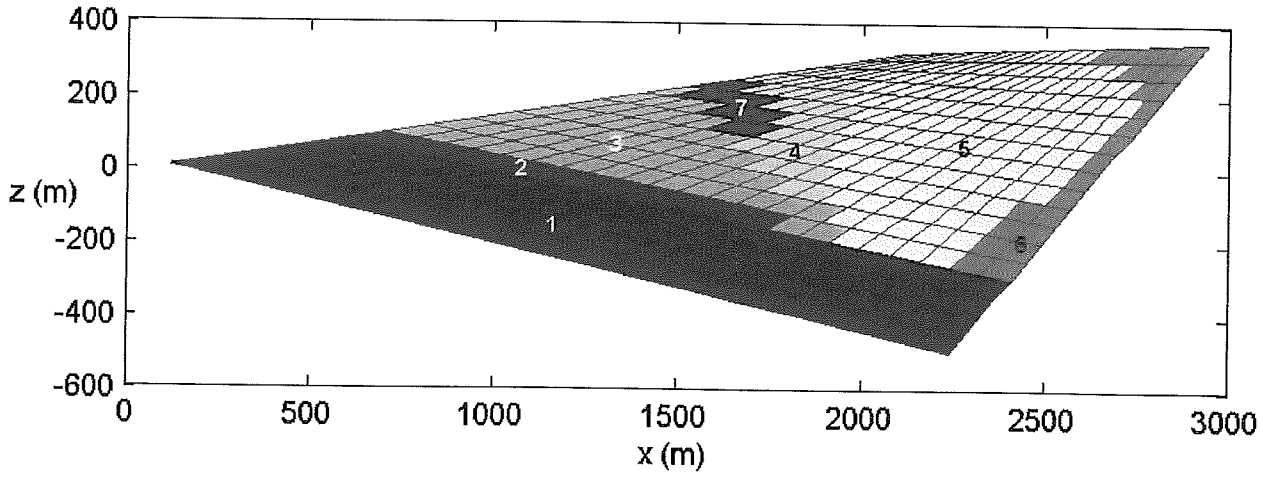

Figure 4.6. The schematisation of the different formations. 1.Kapp Starostin Formation, 2. Vardebukt Formation, 3. Ny-Ålesund Formation, 4. Gipshuken Formation, 5. Wordiekammen and Scheteligfjellet Formation, 6. Brøggertinden Formation, 7. Kapp Starostin Formation.

The values for permeability and porosity of the different formations used in a simulation were based on the values given in Annex 3. The values were reasonably averaged (Table 4.2). The values do not change in x-, y- and z-direction within an element, so each element is isotropic.
The Vardebukt Formation (no. 2 in figure 4.6) acts as an aquitard during the simulation. The Ester mines sometimes penetrate through this aquitard and make a connection with the Kapp Starostin Formation (no 1. in figure 4.6).

Table 4.2. The different formations with the values for permeability and porosity used in the simulation.

No. in Fig. 4.4	*Formation*	*Permeability (m^2)*	*Porosity (-)*
1	Kapp Starostin Formation	$1.0 \cdot 10^{-10}$	0.15
2	Vardebukt Formation	$1.0 \cdot 10^{-16}$	0.05
3	Ny-Ålesund Formation	$1.0 \cdot 10^{-15}$	0.02
4	Gipshuken Formation	$1.0 \cdot 10^{-14}$	0.01
5	Wordiekammen and Scheteligfjellet Formation	$2.0 \cdot 10^{-9}$*	0.05
6	Brøggertinden Formation	$1.0 \cdot 10^{-14}$	0.05
7	Kapp Starostin Formation	$1.0 \cdot 10^{-10}$	0.15

* Value for karstified situation

To provide a connection between the aquifer and the mines during the simulation, a number of elements positioned in the Vardebukt Formation were given the permeability and porosity values of the Kapp Starostin Formation.
For the values for permeability and porosity of the Wordiekammen and Scheteligfjellet Formation, a karstified situation was assumed. As stated in Chapter 2 dolomites and limestones directly underlying glaciers have been reported karstified in other areas on Svalbard and the chemical composition of the water from Ester Spring indicates that long storage times in carbonate rocks are unlikely. Annex E.4 shows a part of the RDARR file with values for permeability.

4.5 Boundary conditions

A numerical model needs boundary conditions to run a simulation. This section will give the boundary conditions that were used during the simulation. The constructed model has 6 boundary surfaces (Figure 4.7).

Boundary surface 1
The boundary condition on surface 1 was set to a no-flow boundary for pressure driven flow and temperatures were specified at the boundary elements, so that conductive heat transport across the boundary was possible.
The underground heat flow in the area is 100 mW/m^2 and this corresponds to a geothermal gradient of 0.035 °C/m (Vågnes *et al.*, 1991).
The values for the temperatures in boundary surface 1 were calculated from the mean annual air temperature (-6.4 °C) in the Ny-Ålesund area (DNMI Klimaavdelingen, 2001) and the geothermal gradient.

Boundary surface 2
This boundary was set to a no-flow situation, for groundwater flow and heat transport. A possible interaction with Austre Brøggerbreen glacier at this boundary cannot be excluded, but there is no information that indicates such interaction. It is assumed that the influence of Austre Brøggerbreen on the groundwater system is small.

Boundary surface 3
The boundary was set to no-flow for pressure driven flow, and a prescribed temperature, allowing conductive heat transport. The temperature at the top of this boundary (z = 350 m) was obtained

from the mean annual air temperature on Zeppelinfjellet (Aas *et al.*, 2001) and the geothermal gradient was used to define the other specified temperatures.

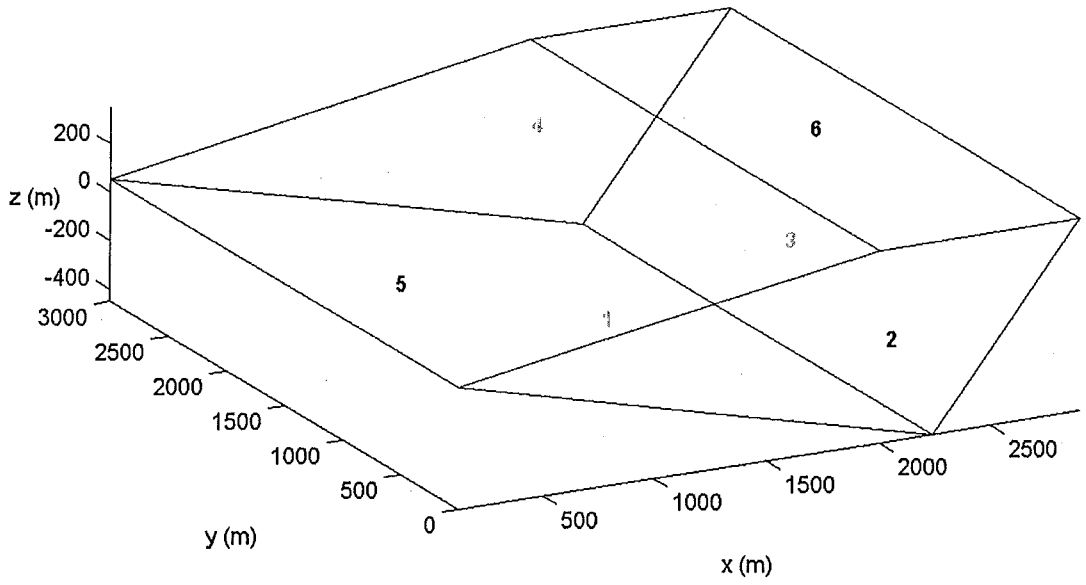

Figure 4.7. Schematic mesh with the six boundary surfaces.

Boundary surface 4
This boundary was set to a no-flow situation, for groundwater flow and heat transport. No data were available that indicate any groundwater or heat flow across this boundary.

Boundary surface 5
As described in section 4.2 this boundary does not follow the groundsurface. The air that was included was filled with formations present at the groundsurface (Figure 4.6). The temperature specified at this boundary was obtained from air temperatures and not from groundsurface temperatures. Temperatures were specified according to the mean annual air temperatures in the Ny-Ålesund area (DNMI Klimaavdelingen, 2001) and on Zeppelinfjellet (Aas *et al.*, 2001).
The boundary was closed for pressure driven flow except for one element that was given a specified pressure to establish the Ester Spring in the model. The specified pressure was calculated iteratively to obtain atmospheric pressure at the inflow point and was set to $2.6 \cdot 10^6$ Pa. The temperature in this element is calculated during a simulation.

Boundary surface 6
The temperature was set to the mean annual air temperature on Zeppelinfjellet (Aas *et al.*, 2001): –7.2 °C. Heat flow across the boundary is possible for this boundary and it is closed for pressure driven flow, except at the infiltration point. At the infiltration point a total mass flux across the

boundary into the system was prescribed. In the area only one recharge area (Vestre Lovénbreen) is present and there is only one discharge point (Ester Spring). There are no data about the amount of water infiltrating into the system. The value used for the infiltration was taken from the measured discharge at the Ester Spring.
The discharge of 700 l/min was recalculated by division of the area of an element, to a value in m/s, because the input needed infiltration in m/s. This gives a total infiltration rate of $2.85 \cdot 10^{-6}$ m/s.
The infiltration occurs over almost the whole width of Østre Centerfelt, which has an averaged width of 1000 m (Booij, 1997). Therefore the infiltration was spread over 1000 m in the y-direction of figure 4.6, which corresponds to 10 elements and an infiltration rate of $2.85 \cdot 10^{-7}$ m/s per element.

4.6 Different variants

With the data and information described in section 4.2, 4.3, 4.4 and 4.5 a base case was constructed. However, during this study, a number of considerations have been important and have been used to construct a number of variants. This section will deal with the variants and the difference of these considerations with the base case.
The considerations, important for the construction of the variants, were:

- The permeability and porosity in the mining area.
- The spatial variation of the infiltration.
- The amount of infiltrating water into the system.
- The interaction between the temperature, viscosity and groundwater flow.
- The construction of the mesh and the consequences of the approximation in section 4.2.

Permeability and porosity in the mining area
In the base case the permeability and porosity in the mining area was not included in the Ny-Ålesund Formation. This means that the water has to flow through the Ny-Ålesund Formation. This formation has a relatively low permeability and porosity and this will influence the velocity of the groundwater flow and the residence time.
In reality the groundwater flows through the mines. To account for this, a variant was made with a higher permeability and porosity for a row of elements (a schematised 'gallery of a mine') in the schematised area of the Ny-Ålesund Formation. This is the lowest row of elements of the Ny-Ålesund Formation in figure 4.6. Another variant was constructed with only a relatively high value for the porosity for the same row of elements. The values are shown in Table 4.3.

Table 4.3. Values for permeability and porosity of the variants.

Variant	*Permeability (m^2)*	*Porosity (-)*
High permeability and porosity	$2.0 \cdot 10^{-9}$	0.1
High porosity	$1.0 \cdot 10^{-15}$	0.1

Spatial variation of the infiltration
In the base case, water flows into the system over a length of 1000 m. However, there are no observations of where the infiltration actually takes place, so variants were made with a different area for infiltration. A variant was made where water infiltrates over half the length of the base case (500 m) and in another over one element (100 m).

The amount of infiltrating water
In the base case the quantity of water infiltrating into the system equals the discharge of Ester Spring. However, the Vestre Lovénbreen is decreasing and so is the recharge of the groundwater system under the glacier (Haldorsen *et al.*, 1999). To account for that a variant was made with

half of the infiltration of the base case: $1.425 \cdot 10^{-7}$ m/s. The infiltration took place over a length of 1000m, as in the base case.
The infiltration was also decreased to $1.425 \cdot 10^{-7}$ m/s for the variant that includes 'the mine gallery' into the Ny-Ålesund Formation.

Interaction of temperature, viscosity and groundwater flow
In a groundwater system where the temperature changes, viscosity changes, and this will influence the groundwater flow.
In the base case the temperature varies from –7.2 °C to 20.8 °C. In this temperature course the viscosity changes from $2.341 \cdot 10^{-3}$ to $1.002 \cdot 10^{-3}$ kg/(m·s) (Weast, 1976). This is a large difference. Due to numerical problems, it was not possible to do a simulation with a temperature dependent viscosity. So, a constant value for the viscosity had to be used. However, to illustrate the effect of the viscosity a variant was created with a different value for the viscosity, compared to the base case: $1.787 \cdot 10^{-3}$ kg/(m·s).

Construction of the mesh and the consequences
As described in section 4.2 a deformed element mesh was constructed. The METROPOL user guide (Sauter *et al.*, 1993) reports that the mesh may be distorted as long as the angles are between 0° and 180°. Booij (1997) uses a distorted element mesh and reports no problems.
However, during the simulations, numerical errors occurred when the viscosity was made temperature dependent.
Although the values of the dispersivities were in accordance with the Péclet criterium, numerical problems still occurred and dispersivities had to be set to a higher value.
Large problems occurred during particle tracking; it was impossible to calculate a 'normal' particle trajectory and a residence time.
To point out the error that occurred during calculation of a particle track, a cubic mesh was made with angels of 90° at all element corners (Figure 4.8). A hypothetical groundwater system equal to the base case was simulated with the use of the cubic mesh. Infiltration occurs at the top of the system and the spring discharges at the same surface boundary as in the base case. Afterwards particle tracking was performed.

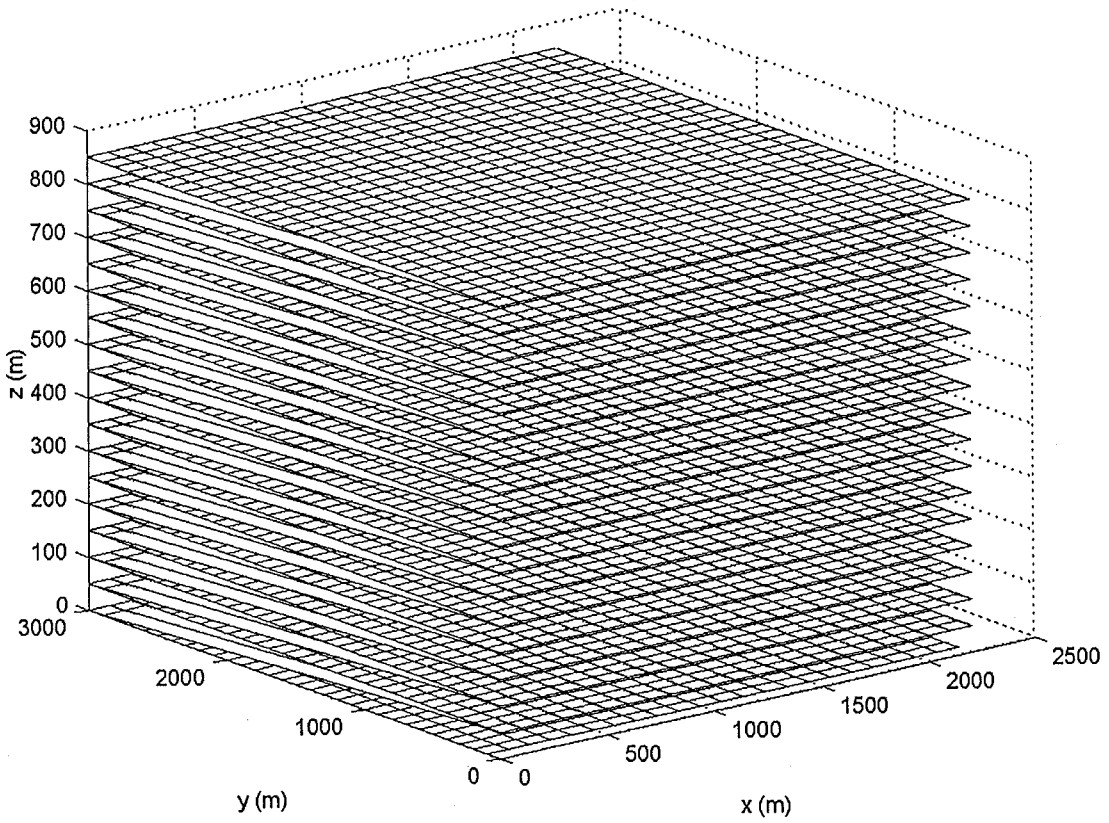

Figure 4.8. The constructed cubic mesh for a hypothetical groundwater system.

4.7 Postprocessing

The output of METROHEAT consist of a file with x, y and z-coordinates and a physical value, pressure, temperature or averaged effective velocity. The values for pressure and temperature are given per node and the values for averaged effective velocity per element.
Postprocessing was done with Matlab Version 6.1, a computer programme for computation, visualisation and programming. With Matlab, surfaces and areas can be plotted. The output file contained data for the whole area and slices were made by extracting a number of data from the output file, before the data were plotted. In Matlab, this kind of procedures can be made in so-called m-files (See annex F). Recalling the m-file will carry out the procedure that is stated in the m-file. Matlab uses bilinear interpolation for plotting data. The data for effective averaged velocity were converted to log velocity in Excel before they were plotted in Matlab.

5 Results and discussion

5.1 Introduction

The results of the simulation are presented in plots of the pressure distribution, temperature distribution and velocity distribution.
In this chapter five different situations will be discussed; a base case and four other situations developed from this base case.

5.2 Base case

The pressure distribution is shown in figure 5.1. Figures with pressure distribution of the other simulations are not included, because the pressure distribution varies little with the different simulations. The pressure distribution is almost hydrostatic for all the simulations.

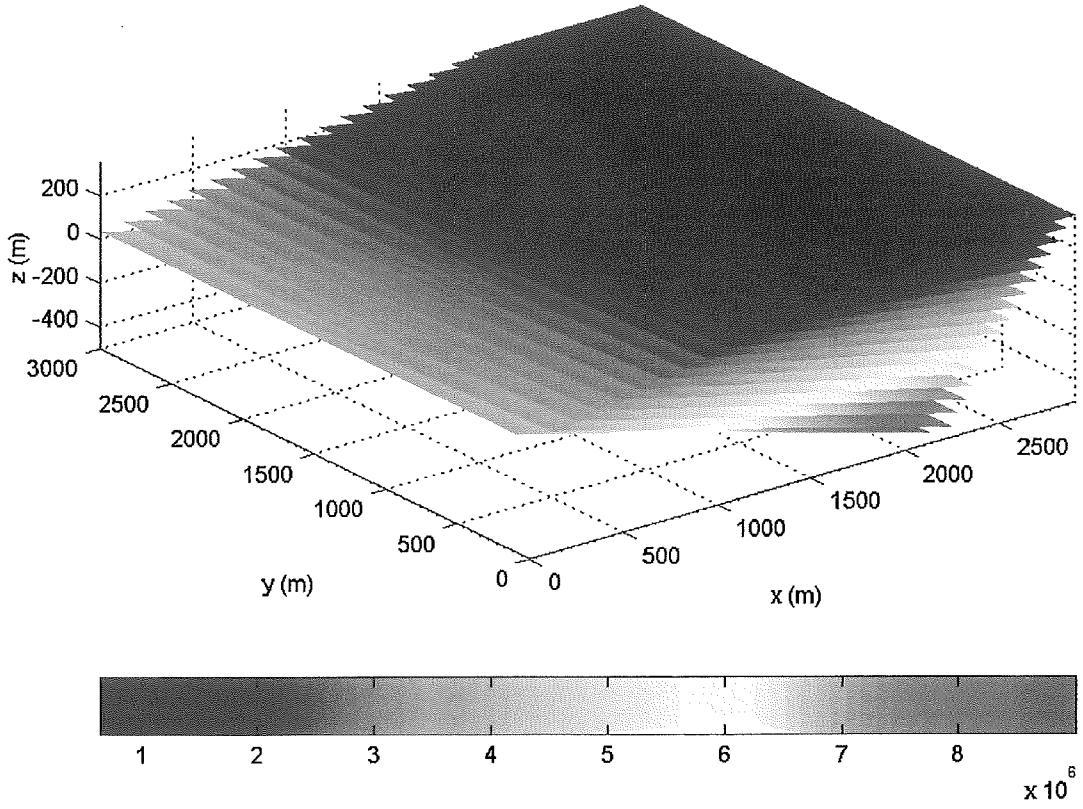

Figure 5.1. The pressure distribution (in Pa) in the base case.

Different xz-slices with the temperature distribution are shown in figure 5.2. The temperature distribution does not change much in the y-direction. This is most likely due to the equality of the distribution of the values for permeability and porosity in the y-direction.
The Ester Spring can be seen in plot *c* at y = 1500 m. The temperature at the outflow point is 1.17 ° C. This is a bit higher than the measured temperature in the field, which was 0.9 °C.

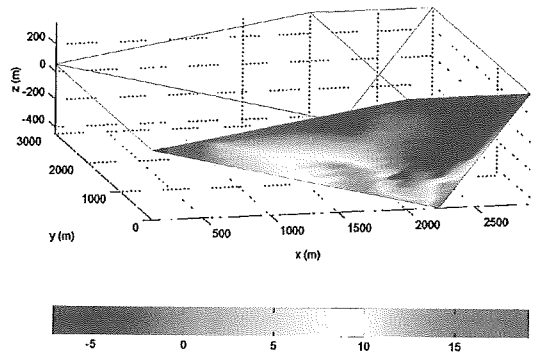

a

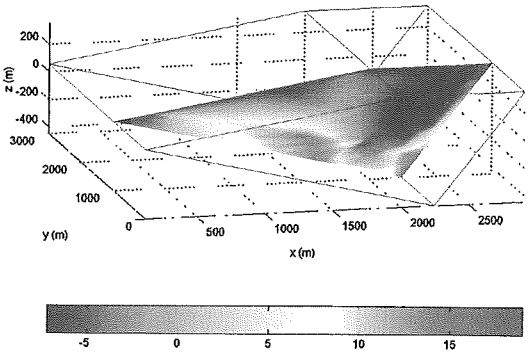

b

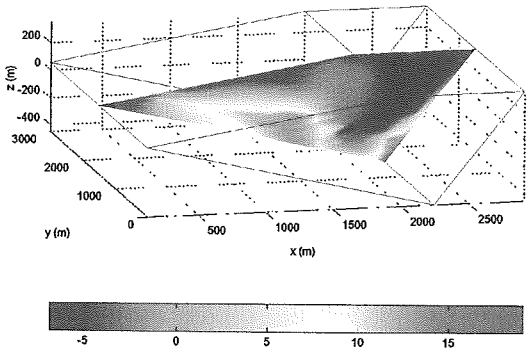

c

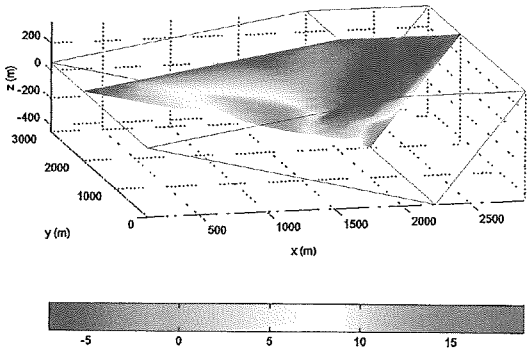

d

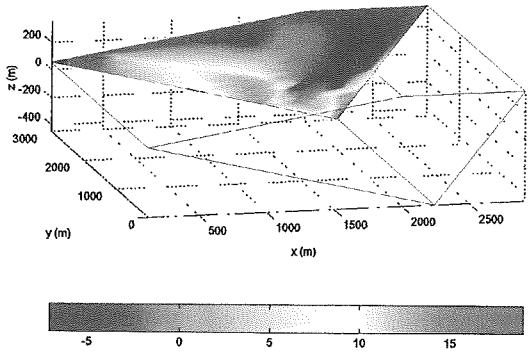

e

Figure 5.2. Temperature distribution (in °C) of xz-slices (a. y = 0 m, b. y = 1000 m, c. y = 1500m, d. y = 2000m, e. y=3000m).

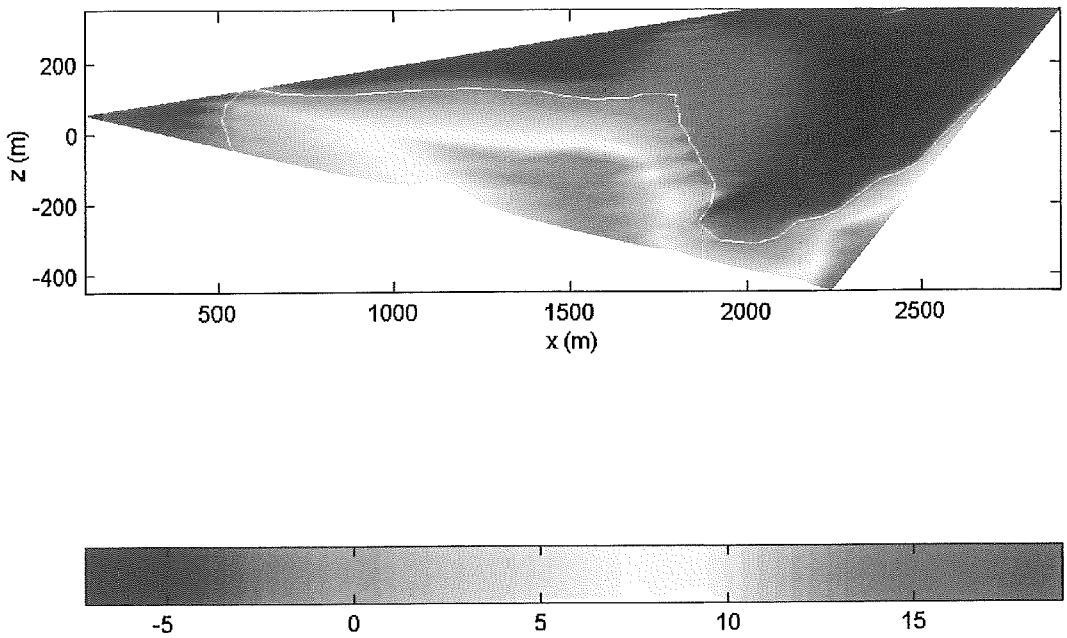

Figure 5.3. Temperature distribution (in °C) of a xz-slice at y=1500m.

Figure 5.3 shows the temperature distribution in xz-direction for y = 1500m. The white contour line indicates the 0 °C contour line. The figure shows the Ester Spring on the left, where the contour line touches the boundary. The water, which infiltrates at the top, has a temperature of 0 °C and it is therefore difficult to distinguish the difference between the 0 °C boundary of the permafrost and the infiltrating water. The infiltrating water flows deeply into the system and when it comes close to the lower boundary in the right part of figure 5.3, it seems to have more influence on the temperature distribution than the geothermal heat. Closer to the Ester mine, the water will have a temperature higher than 0 °C (due to geothermal heating) and the 0 °C contour line will indicate the lower boundary of the permafrost there. In this situation, the permafrost is about 50-200 m deep. This is in agreement with the observed depths in the Ny-Ålesund area (Orvin, 1944, Liestøl, 1977, Haldorsen *et al.*, 1996).
The water infiltrates with a temperature of 0 °C into the system. This cannot be seen in figure 5.3; at the top of the system (at z = 350 m) the temperature is lower than 0 °C. At the boundary a temperature was specified, but the model calculates the heat flux that comes into the system. This heat flux will influence the temperature in the system, but the temperature does not have to be 0 °C. In the real physical system water will not flow with temperatures below 0 °C. Probably the water will flow through some relatively wide and open channels instead of flow through pores. It is possible that the carbonate rocks that underlie the glacier are karstified. In that case there will be no thermal equilibrium between the flowing water and the rock as is assumed in this study.

The groundwater velocity varied in such a way that is was necessary to plot the logarithm of velocity. Figure 5.4 shows the logarithm of total averaged effective velocity.

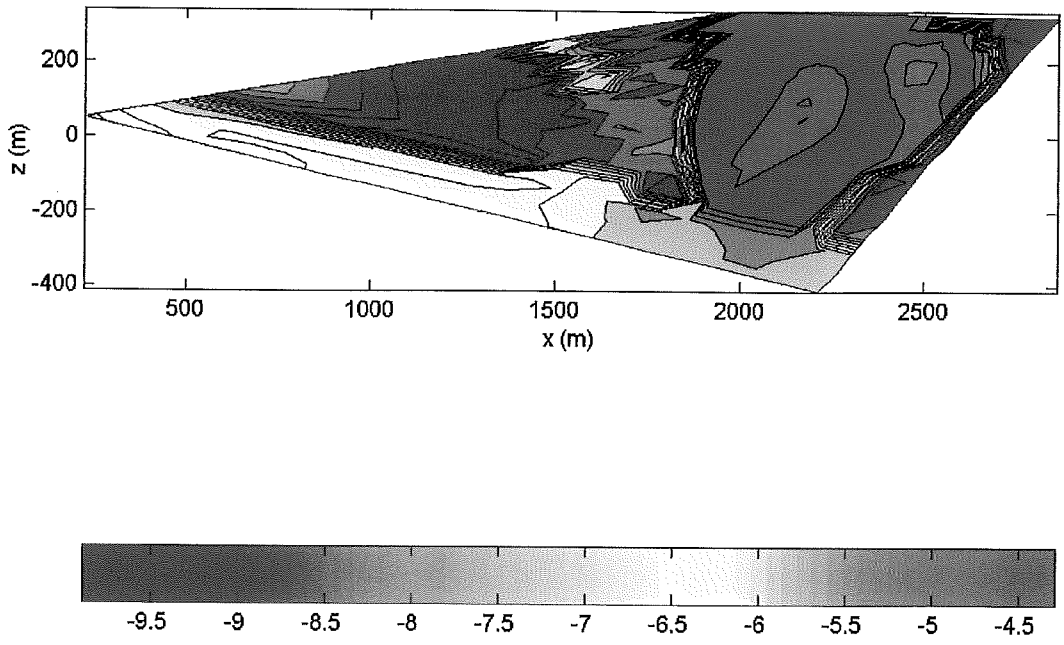

Figure 5.4. Logarithm of total averaged effective velocity (y = 1500 m).

The total averaged effective velocity is calculated by:

$$\bar{v}_{eff} = \sqrt{((\bar{v}_x)^2 + (\bar{v}_y)^2 + (\bar{v}_z)^2)} \qquad \text{[m/s]} \qquad (5\text{-}1)$$

With:

$\bar{v}_{x/y/z}$: The averaged effective velocity in x-, y-, or z-direction.

The figure shows a relatively high velocity in the Wordiekammen and Schetligfjellet Formation, a relatively low velocity in the Kapp Starostin Formation (the aquifer) and the lowest in the Ny-Ålesund Formation. The Wordiekammen and Scheteligfjellet Formation were assumed karstified during this simulation and this is the reason groundwater flows relatively fast through these formations. In this situation, no mines were modelled in the Ny-Ålesund Formation and this explains the relatively low velocity in that area.
It was not possible to calculate particle tracks and residence times; this will be discussed in section 5.7. Instead, an estimate of the residence time was obtained from the velocity distribution along different tracks a particle could take.
This estimate gives residences times of 15000 years. It should be noted that in reality the water will flow through the mines and not through the Ny-Ålesund Formation and this will shorten the residence time. Also the resolution of the constructed grid will be too coarse to calculate residence times properly and the particle will follow a three dimensional track instead of a two dimensional one that was used for the estimate.
The residence time in the karstified limestone is estimated at about 2 years.

5.3 Variation of the permeability (k) and porosity (n) in the mine area

Results of the simulation with a higher permeability and porosity in the mine area are shown in figure 5.6 and figure 5.7.
In figure 5.6 it can be seen that the temperatures in the area of the mines are below 0 °C. The Ester Spring is frozen and the temperature is – 6.5 °C. Permafrost is about 100-200 m deep. The velocity of the groundwater (Figure 5.7) in the area of the mines is lower compared with the velocity in the base case.
The porosity and permeability have higher values than in the base case, but the infiltration and therefore the flux through the system remains equal. The same amount of groundwater can flow through a larger area; therefore it can flow with a lower velocity. This is illustrated in figure 5.5.

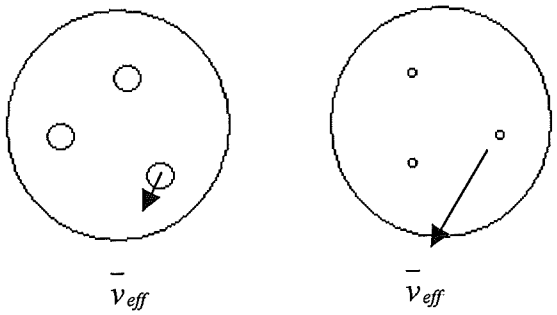

Figure 5.5. Difference in averaged effective velocities due to differences in porosity.

With a lower velocity and an equal flux through the system the heat transport by convection remains equal. But with a higher porosity the heat capacity increases. So, with the same heat transport, but with a higher heat capacity, the temperature will be lower.
Furthermore, it is possible that with a higher porosity the water infiltrating into the system does not flow deeply into the aquifer and the water has a lower temperature when it starts flowing through the permafrost.
The residence time is estimated to 100000 years in this situation. In the carbonate rocks the estimate gives 0.6 years.
A simulation was done with only the higher porosity and the results show the same features in the area of the mines, although less pronounced. It seems the effects intensify when the changes in permeability and porosity are combined.

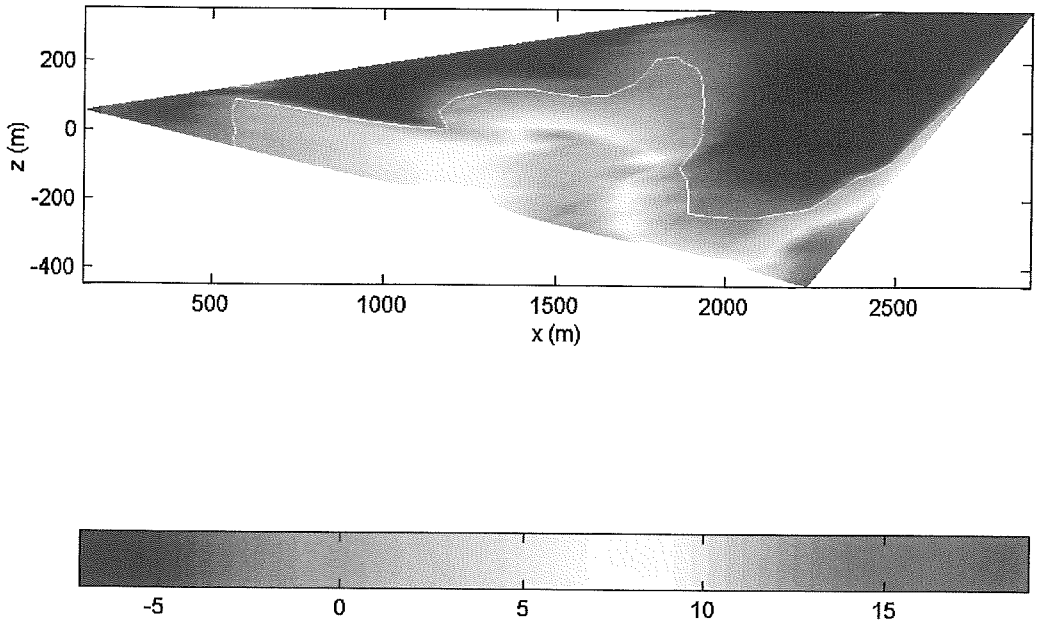

Figure 5.6. Temperature distribution (in °C) with high permeability and porosity (y=1500m).

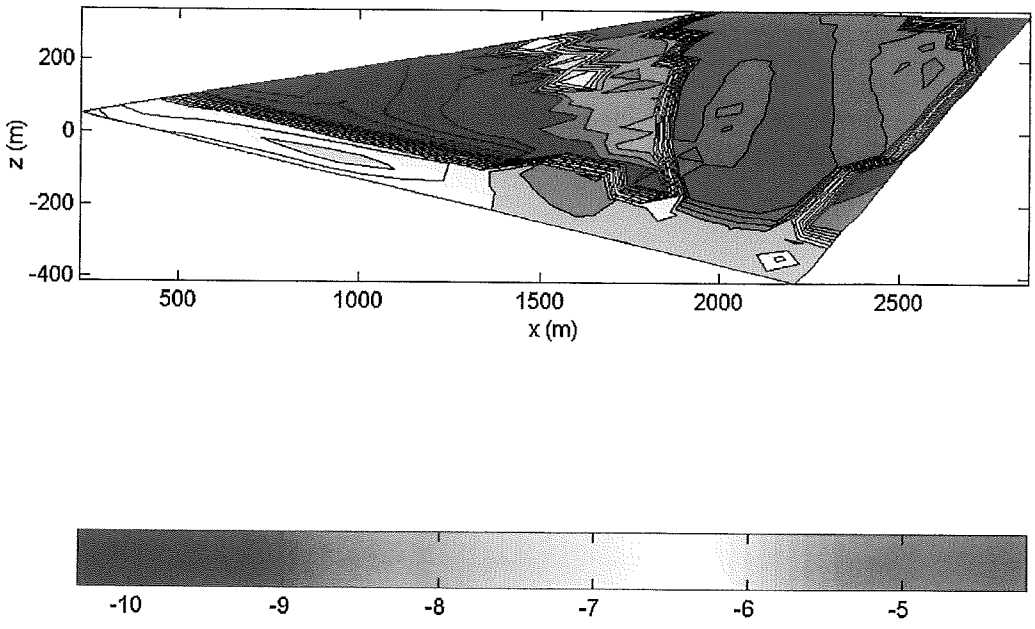

Figure 5.7. Log of velocity with high permeability and porosity (y=1500m).

5.4 Spatial variation of the infiltration

The simulations where the infiltration varied spatially over 500 and 100 m show no extreme differences and it was difficult to compare these differences. To illustrate the difference, the data of the base case were abstracted from data of the variants with infiltration over 500 and 100 m. This resulted in figures 5.8 and 5.9. For the figures the results of the temperature distribution were used, comparisons with the results of the velocity distribution give the same indications as the comparison with temperature data. The comparison of the velocity distribution is not shown.
Figure 5.8 shows the differences between the variant with an infiltration over 500m and the base case. Figure 5.9 shows the differences between the variant with an infiltration over 100m and the base case. The permafrost depth is the same as in the base case: 50-200 m deep. An estimate of the residence times gives 35000 years for the situation with infiltration over 500 m and 26000 years for the situation with infiltration over 100 m. Estimated residence times in the carbonate rocks are 0.8 and 1.1 year for infiltration over 500 m and 100m respectively.
The differences in the estimate of the residence time are likely due to the inaccuracy of the estimate procedure.
The largest differences occur at the infiltration point and in the Wordiekammen and Sheteligfjellet Formation. This can be expected since this area is closest to the infiltration point and the groundwater flows relatively fast through these rocks. The influence of the spatial variation of the infiltration at the Ester Spring is negligible.
The largest difference occurs between the variant with an infiltration over 100m and the base case. This can be expected since these two situations differ most. However, the influence on Ester Spring is still negligible.

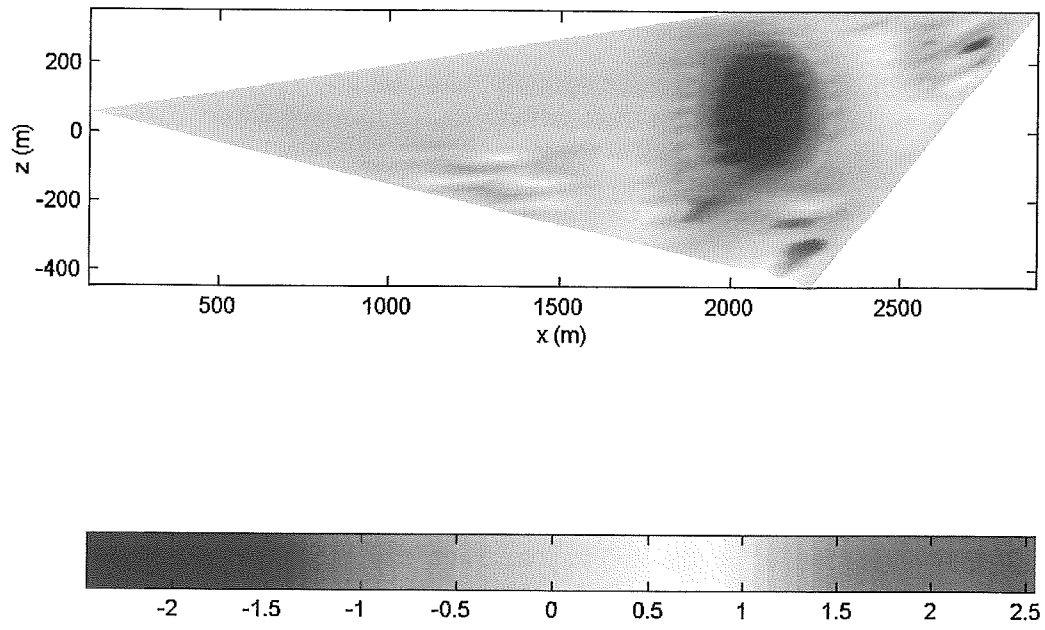

Figure 5.8. Difference in temperature (in °C) between base case and situation with infiltration over 500 m (y=1500m).

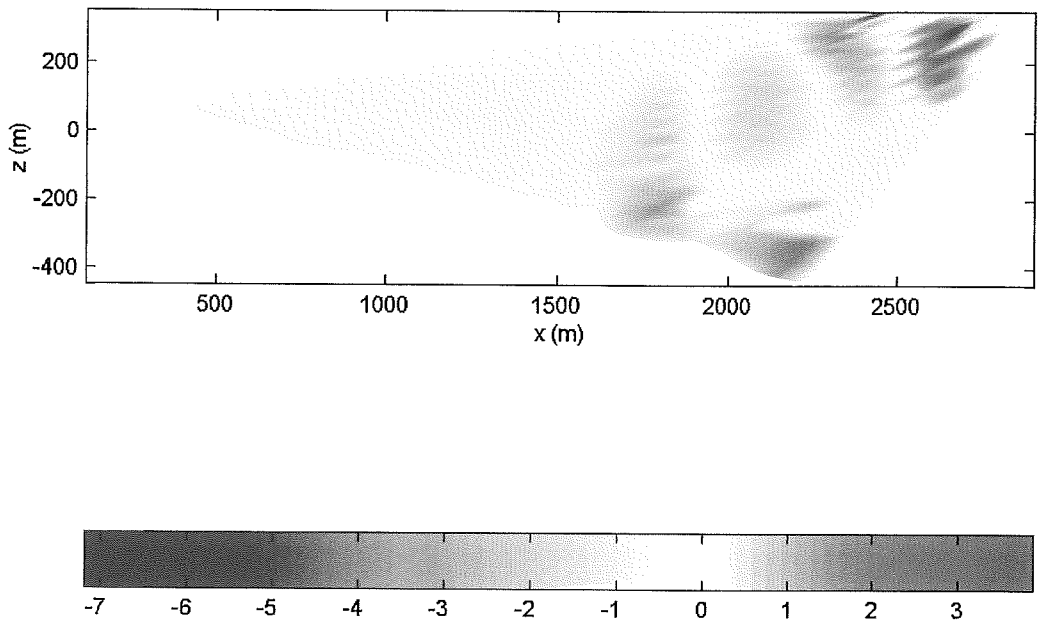

Figure 5.9. Difference in temperature (in °C) between base case and situation with infiltration over 100 m (y=1500m).

5.5 Variation in the amount of the infiltration

The results of the variant with half of the infiltration are shown in figure 5.10 and 5.11. The results of the variant with half the infiltration and the presence of 'a gallery of a mine' are shown in figure 5.12 and 5.13.
In the variant with half of the infiltration, there is still a large impact on the in inflowing water on the temperature distribution, especially in the Wordiekammen and Scheteligfjellet Formation. However, the temperatures in the aquifer are higher than in the base case. Also, the temperature at Ester Spring is higher: 1.92 °C. The permafrost thickness is about 50-200 m.
With less water of 0 °C that infiltrates into the system and the same amount of energy that comes from geothermal heat, the groundwater will get a higher temperature when it flows through the system.
The velocity of the groundwater in the different formations is lower than in the base case. With less infiltration, the flux through the saturated groundwater system will decrease and this explains the lower velocity.
In the simulations the system remains saturated, although the flux decreases. But a decrease in recharge in the real system, may lead to unsaturated conditions in the groundwater system under Vestre Lovénbreen, and such a system will act differently than the simulated one.
An estimate of the residence time of water in the system gives 32000 years, in the carbonate rocks 1.28 years.

In the simulation with the variant with half of the infiltration of the base case and an adapted value for permeability and porosity in the area of the mines, also higher temperatures occur in the aquifer. The difference with figure 5.10 is that the Ester Spring is frozen, just as in figure 5.5 in section 5.3. The temperature at the Ester Spring is –6.5 °C. The permafrost depth is 45-200 m.
The influence of the different values for permeability and porosity is more dominant in the mine area than the groundwater flux.
The velocity of the groundwater in the mine area is lower than in the base case. An explanation for the low velocity in the mine area and the frozen spring has been given in section 5.3.
The estimated residence time is about 100000 years for the entire system, for the carbonate rocks 0.6 year.

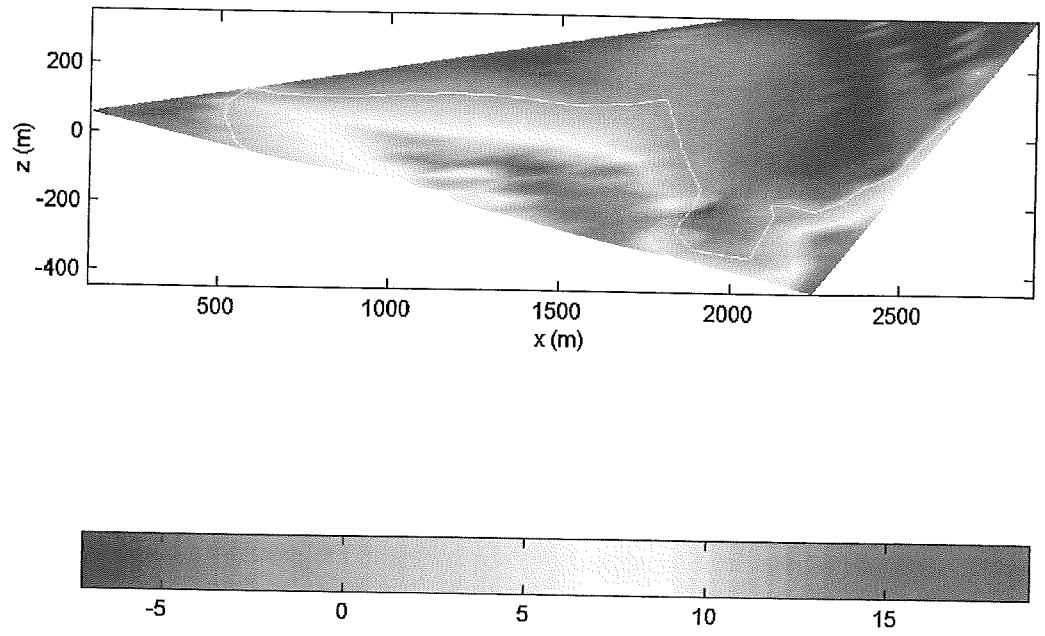

Figure 5.10. Temperature distribution (in ºC) with half of the infiltration (y=1500m).

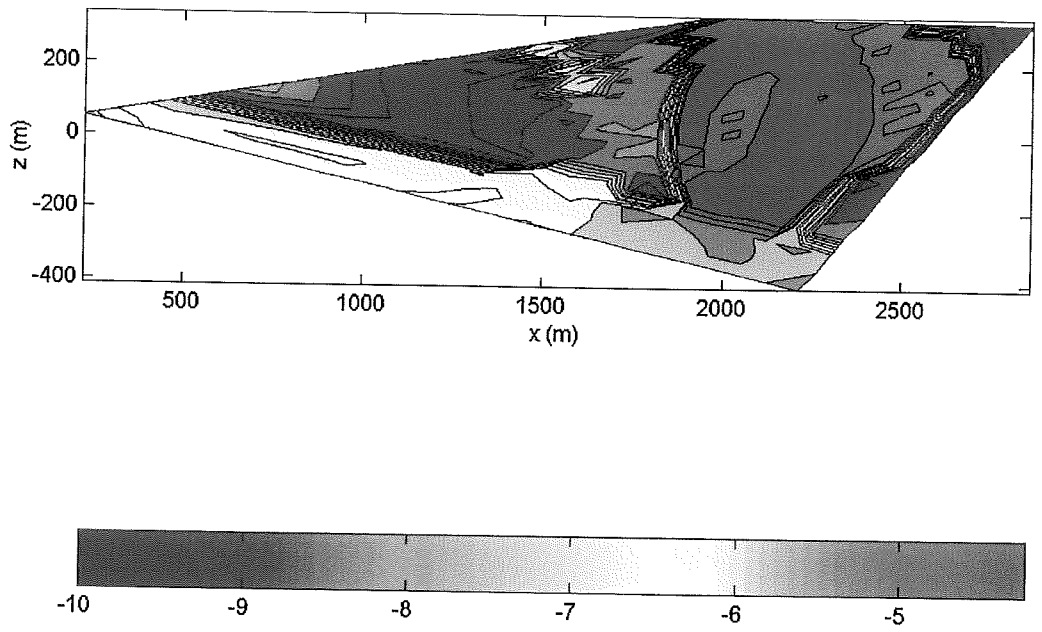

Figure 5.11. Log of velocity with half of the infiltration (y=1500m).

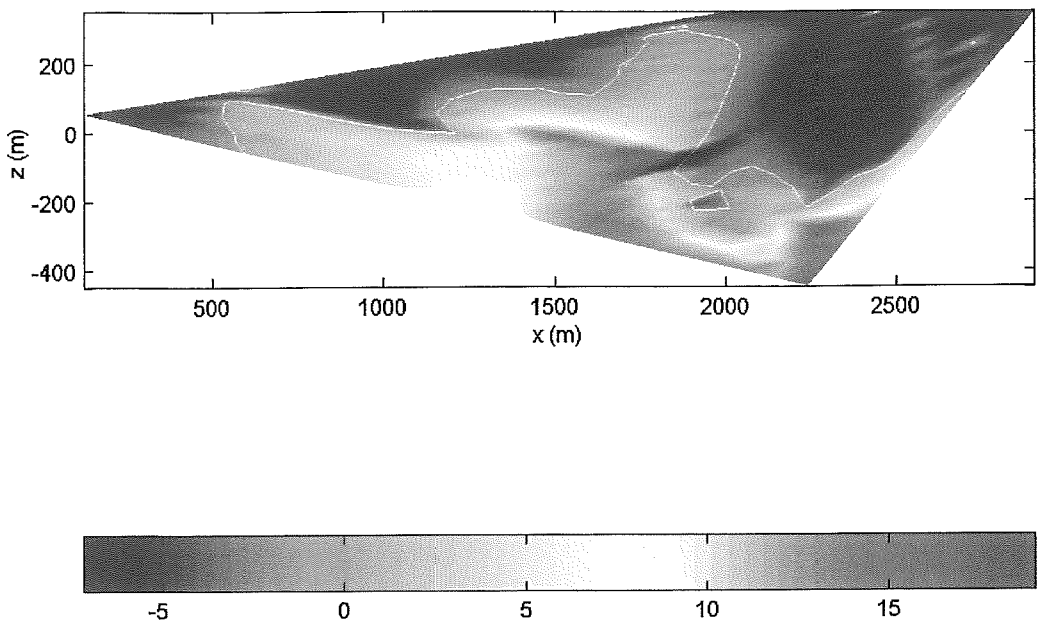

Figure 5.12. Temperature distribution with half infiltration and included mine area (y=1500m).

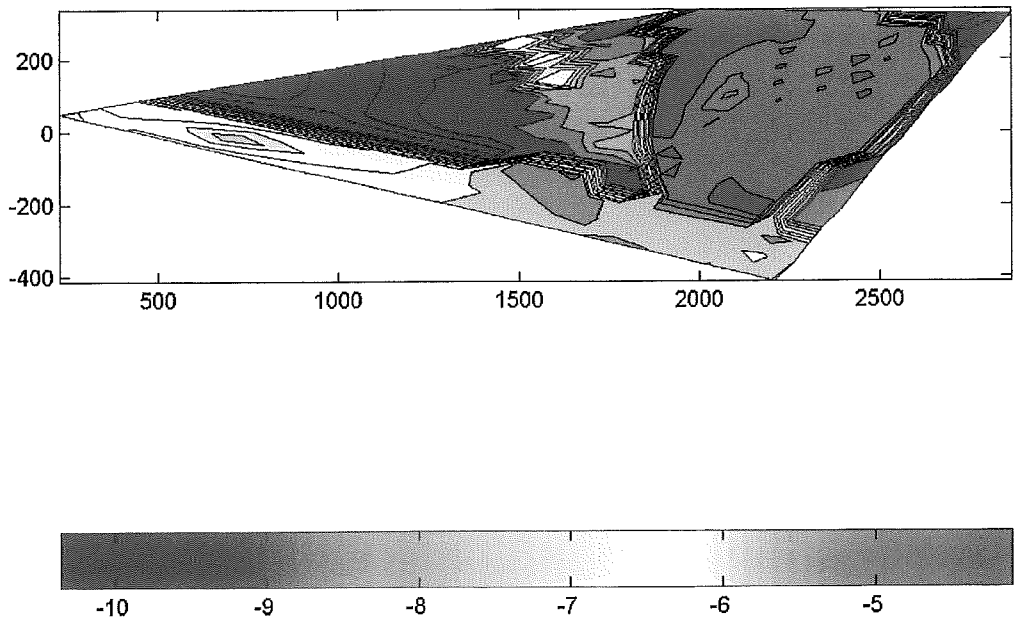

Figure 5.13. Log of velocity with half infiltration and included mine area (y=1500m).

5.6 Different value of viscosity

The temperature distribution of the variant with a higher value for the viscosity is shown in figure 5.14. It shows an increased area with a temperature above 0 °C. The velocity (in figure 5.15) is lower than in the base case. The temperature at the Ester Spring is 0.75 °C, lower than in the base case. The simulated permafrost layer is about 45-175 m deep. An estimate for the residence time gives 44000 years. For the carbonate rocks the estimate gives about 0.8 year.

The variant with a higher viscosity was simulated to illustrate the importance of this parameter on a groundwater system that is influenced by heat flow, especially when the temperatures have a range as in these simulations. Regrettably, the viscosity could not be taken into account due to numerical problems. The numerical problems will be discussed in section 5.7.

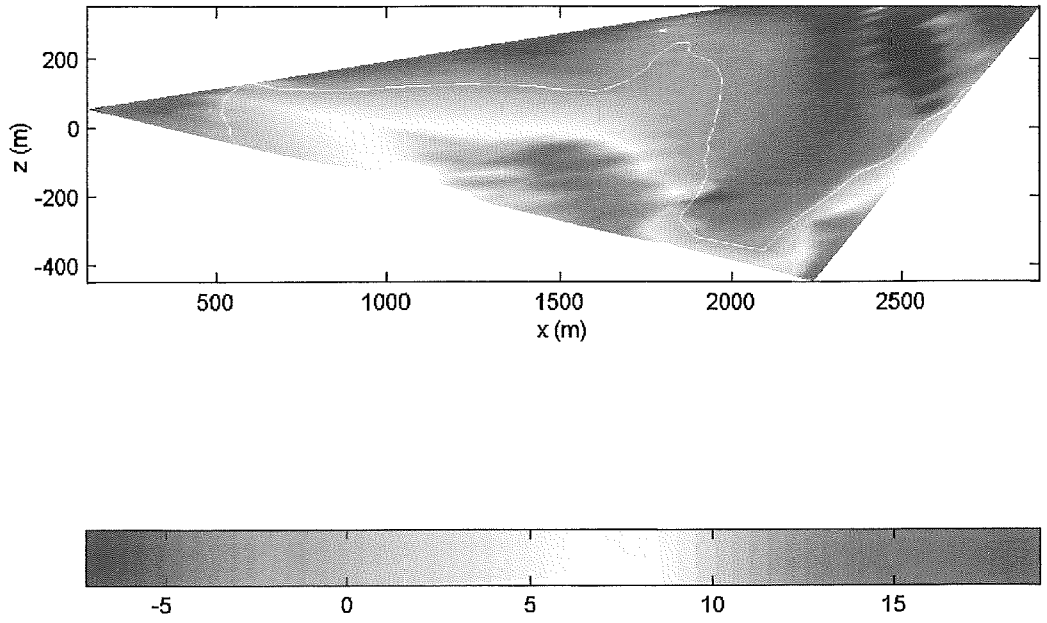

Figure 5.14. Temperature distribution with a different value for liquid viscosity (y=1500m).

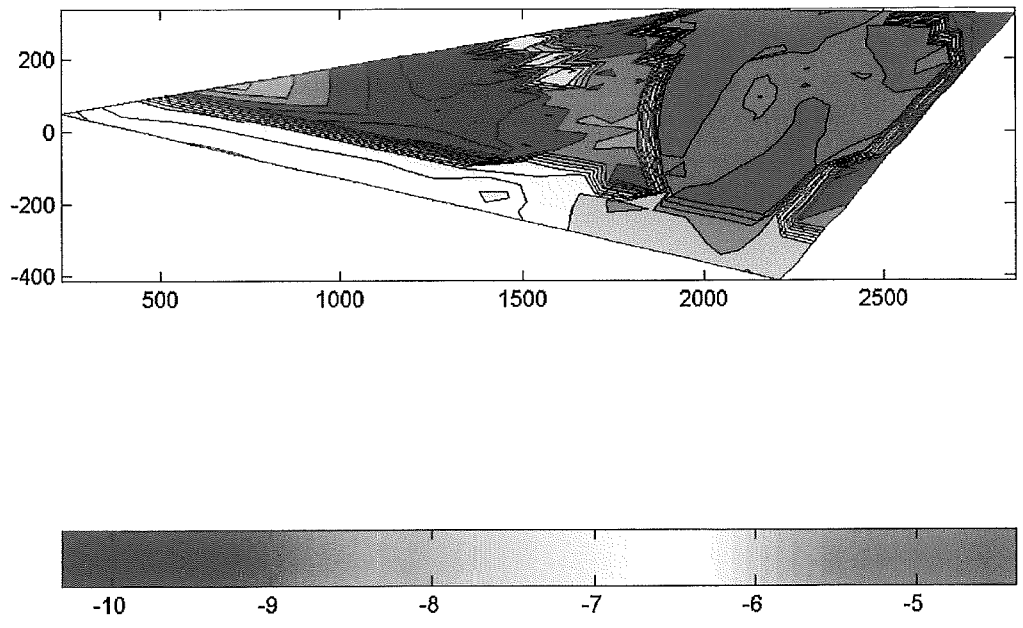

Figure 5.15. Log of velocity with a different value for liquid viscosity (y=1500m).

5.7 Particle tracking

Figure 5.16 shows a particle trajectory that is calculated in the base case. It is very unlikely that a particle would follow such a trajectory in a groundwater system.
METROPOL uses local velocities to calculate a particle trajectory and the residence time of the particle. In the base case, the local velocity field is erroneous if a particle follows a trajectory as shown in figure 5.16.
For the calculation of the temperature however an averaged velocity in an element is used. This averaged velocity is used in the calculation of the heat flux in x-, y- and z- direction, $\rho c_f Tq$ in the energy mass balance equation (see section 3.3.1).
When the local velocities in an element are averaged, the errors appear to cancel out.
Therefore, the calculated temperatures and the averaged effective velocity values are still reasonable in this study, although the local velocity field is erroneous.
This holds as long as the errors in the local velocity filed are not too big. When, for instance, the viscosity was made dependent on the temperature, the errors in the local velocity field increased, and they were not cancelled during averaging. These errors could be seen in the temperature and averaged effective velocity distribution.
The errors in the local velocity field were caused by the chosen discretisation of the mesh. The elements were deformed in such a way that METROHEAT could not calculate the local velocity field in the right way, although MMESH and METROHEAT mention the possibility to use a deformed mesh.
Figure 5.17 illustrates a particle trajectory that was calculated in the hypothetical groundwater system. In this simulation, a straight mesh was used. A particle flows from the infiltration area towards the spring. This particle has no strange paths or curls in its trajectory and is believed to be correct.
It is beyond the scope of this research at what angle in an element numerical errors would occur. The angles in the mesh used for the Vestre Lovénbreen groundwater system go up to 170 °. Leijnse (1992) reports about numerical errors in a deformed elements with an angle higher than 120°, but the model in his report differs from the model for Vestre Lovénbreen and it cannot be concluded that numerical errors will disappear when the deformed mesh has angles below 120°.
METROHEAT has an option to inactivate elements (Leijnse, 1992) and it would be best if elements were made as cube-shaped as possible and to inactivate 'empty elements' to reduce numerical errors.

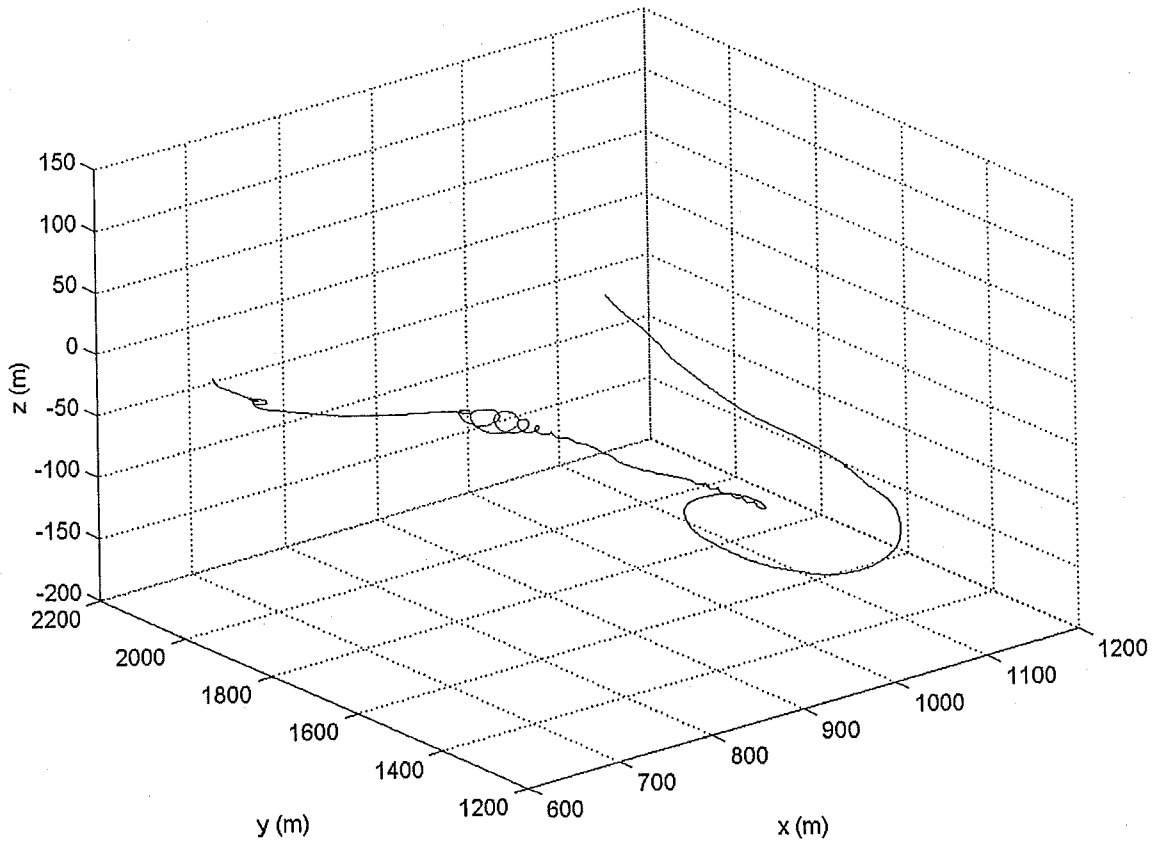

Figure 5.16. Particle trajectory in the base case.

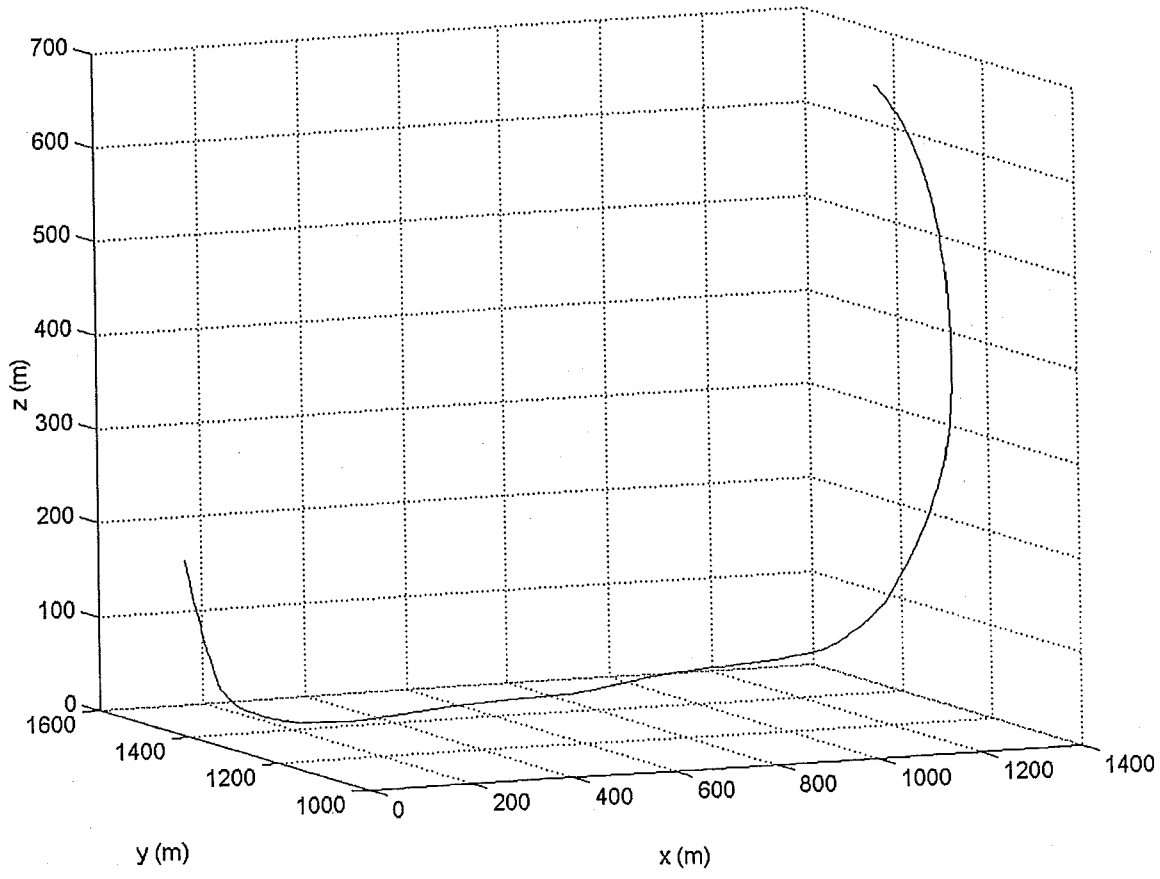

Figure 5.17. Particle trajectory of a simulation with a straight mesh.

6 Conclusions and Recommendations

6.1 Introduction

This study about the groundwater system under Vestre Lovénbreen on Spitsbergen has been a surveying one and the hydrogeological model was simplified in many ways. None of the simulation results will fully resemble the actual groundwater system and lack of data makes it impossible to evaluate the results in a proper way. However, the results presented in chapter 5 are indicative for the response of the real system.
Based on the results that were obtained, a number of conclusions can be drawn. They will be stated in section 6.1. The recommendations will be given in section 6.2.

6.2 Conclusions

- The simulated temperatures at the outflow point are 0.75-1.92 °C. These temperatures lie close to the measured temperature of the spring: 0.9 °C.
- The simulated depth of the permafrost is between 45 and 200 m and this corresponds to the data observed in the field (Orvin, 1944, Liestøl, 1977).
- The temperature distribution in the top of the system supports the idea that water flows through relatively wide and open channels in the carbonate rocks.
- The estimated residence times are in the order of 15000-45000 years, but they are very debatable, because the estimate used in chapter 5 is very rough.
- The velocities of the groundwater in the karstified rock are very similar in the different simulations and the residence time is estimated to be 0.6-2 years. This is in agreement with the chemical composition of the water at Ester Spring that indicates short residence times in carbonate rocks.
- In a flux controlled system, the permeability and the porosity will determine the flow velocity in the different rocks. A higher porosity will give more space for the flowing water and the velocity will decrease. A higher permeability seems to enhance the effect that a higher porosity has on the groundwater system under Vestre Lovénbreen.
- The location where water infiltrates into the ground under the Vestre Lovénbreen has very little influence on the behaviour of Ester Spring. The location will however be important for the trajectories the water will follow and therefore the residence time in the system.
- With a decrease in infiltration of 50%, the Ester Spring did not freeze during the simulations. On the contrary, the simulated outflow temperature was higher when the infiltration into the system was decreased.
- In a saturated system, the flux and the pressure gradient will control the system. In a real system a decrease of infiltration could lead to an unsaturated situation and this will influence the pressure gradient, the velocity and the uptake or loss of energy of the water in the system.
- The value of the viscosity has a large influence on the groundwater flow and the temperature distribution in the groundwater system under the Vestre Lovénbreen.

- The influence of a deformed element mesh on the numerical errors in the local velocity field should not be underestimated.

6.3 Recommendations

- The Ester Spring and the Vestre Lovénbreen should stay monitored to see what happens in the future with concern to the climatic changes.

- A mass balance of the Vestre Lovénbreen should be made. Together with the precipitation data, the infiltration into the system can then be determined. During the simulations in this study a steady state situation was assumed. This assumption can be true for the discharge at Ester Spring, but for the infiltration this assumption is probably not true. Data of the mass balance will give information whether the infiltration can be considered a steady state situation. Also transient simulation can be performed with mass balance data from Vestre Lovénbreen.

- It would be interesting to know the occurrence and the amount of fractures in the different formations. With this information, a simulation with a dual porosity model could be made. With such a model it would also be interesting to model the system without a thermal equilibrium between the water and the rock. However, without information about the fractures, it is useless to consider a dual porosity model.

- A preprocessing program for METROHEAT should be found.

- The mesh constructed with METROHEAT should be as straight as possible, to diminish numerical errors. Empty cells can be made inactive by giving them a permeability value of zero. With the results of a simulation in a straight mesh, a proper particle track can be performed and this will give more information about the residence times within the system. In addition, the mesh should be refined, with smaller elements than used in this study.

- The geology in the y-direction should be taken into account. This will make the system 3-dimensional in the hydrogeological point of view, and it will influence the groundwater flow during the simulation.

- During simulation of the Vestre Lovénbreen groundwater system, the viscosity should be made temperature dependent. The change of the viscosity is too large to not consider it.

- To see what will happen if the system becomes unsaturated due to a decrease in infiltration, a simulation with a model that can handle unsaturated and saturated coupled groundwater flow should be made.

References

Aas, W.,Tørseth, K., Solberg, S.,Berg, T.,Manø, S.,Yttri, K.E. 2001. 'Overvåkning av langtransportert forurnset luft og nedbør', *Atmosfærisk tilførsel, 2000*, NILU OR 34/2001.

Bergh, S.G., Maher,Jr., H.D., Braathen, A. 2000. 'Tertairy divergent thrust directions from partitioned transpression, Brøggerhalvøya, Spitsbergen', *Norks Geologisk Tidsskrift*, **80**, pp 63-81.

Booij, M.J. 1997. 'Simulation of coupled water flow and heat transport of a groundwater system on Spitsbergen', *MSc thesis*. Wageningen Agricultural University and Agricultural University of Norway, 52 pp.

Booij,M., Leijnse, A., Haldorsen, S., Heim, M. 1998. 'Subpermafrost Groundwater Modelling in Ny-Ålesund, Svalbard', *Nordic Hydrology*, **29**, pp 385-396.

Challinor, A. 1967. 'The structure of Brøggerhalvøya, Spitsbergen', *Geological magazine*, **104**, pp 322-336.

Dallmann, W.K. (ed.),1999. 'Lithostratigraphic Lexicon of Svalbard, Upper Paleozoic to Quartenary bedrock', *Review and recommendations for nomenclature use*. Statigrafisk Komité Svalbard (SKS), Norsk Polarinstitutt, Tromsø, 318 pp.

DNMI Klimaavdelingen, 2001. 'Middeltemperatur Ny-Ålesund II'. DNMI, Oslo.

Everdingen, R.O. van. 1997. 'Artic water resources management, Groundwater in the permafrost region' , The Arctic Institute of North America, The University of Calgary, Calgary, Alberta, Canada, 47 pp.

Haldorsen, S., Lauritzen, S.-E., 1993. 'Subpermafrost Groundwater in Spitsbergen', *Hydrology of hard rocks* (XXIVth I.A.H. Mem. Congress), Ås, Norway, pp 940-949.

Haldorsen, S, Heim, M, Laurtizen, S.-E. 1996. 'Subpermafrost Groundwater, Western Svalbard', *Nordic Hydrology*, **27**, pp 57-68.

Haldorsen, S., Heim, M. 1999. 'An Arctic Groundwater System and its Dependence upon Climatic Change: An example from Svalbard', *Permafrost and periglacial processes*, **10**, pp 137-149.

Hanssen-Bauer, I., Kristensen Solås, M., Steffensen, E.L. 1990. 'The climate of Spitsbergen' *DNMI-rapport 39/90 KLIMA*. Det Norske Meteorologiske Institutt, Oslo, 40 pp.

Hassanizadeh, S.M. 1986. 'Deriviation of basic equations of mass transport in porous media, Part 2. Generalized Darcy's and Fick's laws', *Advances in water resources*, **9**, pp207-222.

Hassanizadeh, S.M., Leijnse, A. 1995. 'A non-linear theory of high-concentration-gradient dispersion in porous media', *Advances in water resources,* **18**, pp. 203-215.

Hjelle,A., Lauritzen, Ø. 1982. 'Geological map Svalbard 1:500000, Sheet 3G, Spitsbergen northern part', *Skrifter Nr. 154C*. Norsk Polarinstitutt, Oslo, 15 pp.

Hjelle, A. 1993. 'Geology of Svalbard', *Polarhåndbok no. 7*. Norsk Polarinstitutt, Oslo, 162 pp.

Hisdal, V. 1985. 'Geography of Svalbard', *Polarhåndbok no. 2.* Norsk Polarinstitutt, Oslo, 75 pp.

Hongve, D. 1987. 'A revised procedure for discharge measurement by means of the salt dilution method', *Hydrological Processes*, Vol. 1, pp 267-270.

Isaksen, K. 2001. 'Past and present ground thermal regime, distribution and creep of permafrost-case studies in Svalbard, Sweden and Norway', *PhD Thesis*, University of Oslo, Norway, 48 pp.

Larsen, E., Sejrup, H.P., Olsen, O., Miller, G.H. 1991. 'Late Quartenary Land-Sea Interactions: Fennoscandia and Svalbard-The Nordic Seas', *Quartenary International Vol. 10-12*, pp 151-159.

Lauritzen, S.E. 1990. 'Groundwater in cold climates: interaction between glacier and karst aquifers', *Arctic hydrology: Present and future tasks*, Norwegian National Committee for Hydrology Report **23**, pp. 139-146.

Lefouconnier, B., Hagen, J.O., Ørbæk, J.B., Melvold, K., Isaksson, E. 1999. 'Glacier balance trends in the Kongsfjorden area, western Spitsbergen, in relation to the climate', *Polar Research*, **18(2)**, pp 307-313.

Leijnse, A., 1992. 'Three-dimensional modelling of coupled groundwater flow and transport in porous media' *PhD Thesis*, Department of Civil Engeneering and Geological Sciences, University of Notre Dame, Indiana, 251 pp.

Liestøl, O. 1977. 'Pingos, springs and permafrost in Spitsbergen', *Årbok 1975*, Norsk Polarinstitutt, Oslo, Norway, pp 7-29.

Liestøl, O. 1980. 'Permafost conditions in Spitsbergen: Frost actions in soils' Publication No 21, Oslo, Norway, pp 23-28.

Orvin, A. 1934. 'Geology of the Kings Bay region, Spitsbergen', *Skrifter om Svalbard og Ishavet*, **57**, 195 pp.

Orvin, A. 1944. 'Litt om kilder på Svalbard', *Norsk geografisk tidskrift*, Vol. 10, pp 16-38.

Paterson, W.S.B. 1981. 'The physics of glaciers (2nd Edition)', Pergamon Press, Oxford, 380 pp.

Sauter, F.J., Leijnse, A., Beusen, A.H.W. 1993. 'Metropol, User's guide', RIVM, Bilthoven, The Netherlands

Shaw, E.M. 1994. 'Hydrology in practise', Chapman & Hall, Londen, United Kingdom, 569 pp.

Tolstikhin, N.I., Tolstikhin, O.N. 1976. 'Groundwater and surface water in the permafrost region', *Technical bulletin no. 97*, Inland waters directorate, water resources branch, Ottawa, Canada, 25 pp.

Vågnes, E., Amundsen, H.E.F. 1991. 'Late Cenozoic uplift and volcanism on Spitsbergen; caused by mantle convection?', *Geology*, Vol. 21, pp 251-254.

Weast, R.C. 1976. 'Handbook of chemistry and physics', CRC Press Inc., Cleveland, Ohio.

Annex A Geological Time Table

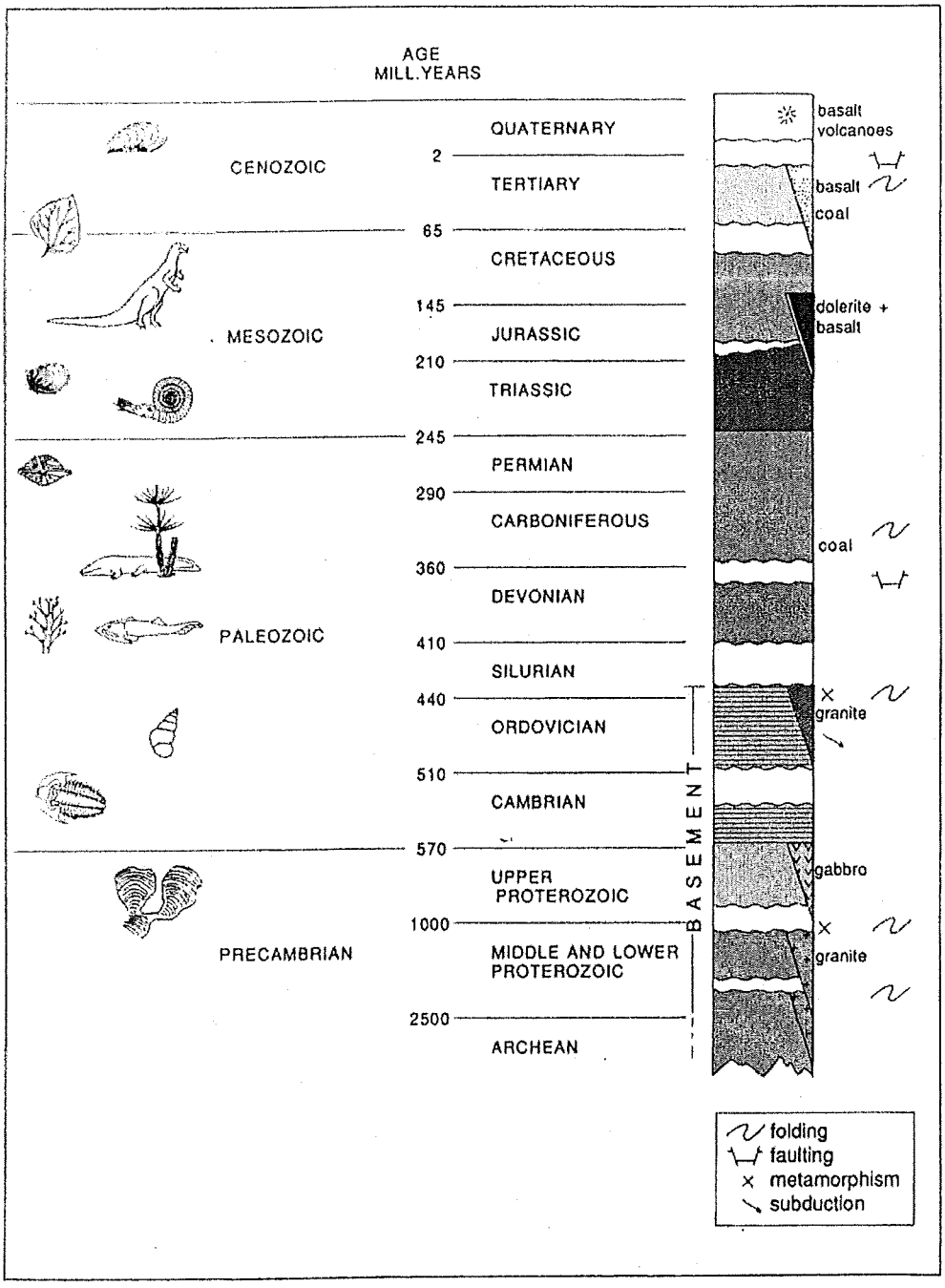

Annex B Geological map of Svalbard (Hjelle, 1993)

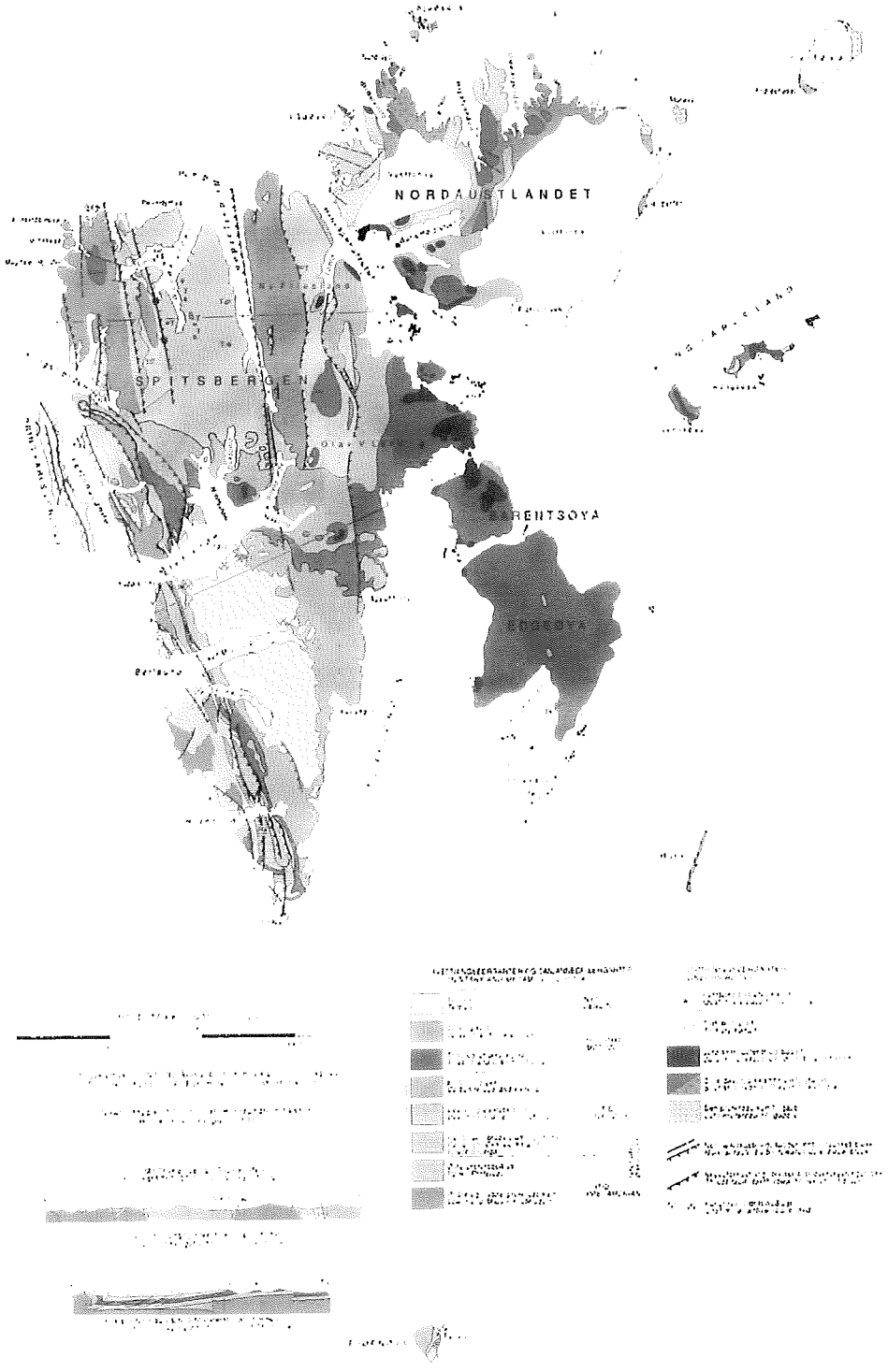

Annex C Geology of the Ny-Ålesund area

Table C.1 Geology of the Ny-Ålesund area with formation names, estimated thickness, rock type, porosity and permeability (Booij, 1997; Booij et. al., 1998; Dallman et. al., 1999, Bergh et. al., 2000).

Period	*Formation*	*Code*[4]	*Thickness (m)*	*Rock type*	*Porosity(-)*	*Permeability (m^2)*
Tertiary	Ny-Ålesund	T-16	>195	sandstone, shales, coal seams	0.02-0.03[3]	$3\cdot10^{-17}$-$6\cdot10^{-13}$[2]
Lower Triassic	Vardebukta	M-02	0-50	shale, siltstone	0.0-0.10[1,2,3]	$1\cdot10^{-20}$-$2\cdot10$-16[1,2,3]
Permian	Kapp Starostin	CP-79	200	glauconitic sandstone, cherts	0.12-0.19[3]	$3\cdot10^{-17}$-$5\cdot10^{-11}$[1,2,3]
	Gipshuken	CP-60	146	dolomite	0.01-0.15[2,3] (0.001-0.05 [2])	$1\cdot10^{-13}$-$2\cdot10^{-9}$[1,2,3] ($1\cdot10^{-16}$-$6\cdot10^{-13}$[1,2,3])
	Wordiekammen	CP-47	290	limestone	0.01-0.15[2,3] (0.001-0.05 [2])	$1\cdot10^{-13}$-$2\cdot10^{-9}$[1,2,3] ($1\cdot10^{-16}$-$6\cdot10^{-13}$[1,2,3])
Carboniferous	Wordiekammen	CP-47		limestone	0.01-0.15[2,3] (0.001-0.05 [2])	$1\cdot10^{-13}$-$2\cdot10^{-9}$[1,2,3] ($1\cdot10^{-16}$-$6\cdot10^{-13}$[1,2,3])
	Scheteligfjellet	CP-36	150	limestone, siltstone	0.01-0.15[2,3] (0.001-0.05 [2])	$1\cdot10^{-13}$-$2\cdot10^{-9}$[1,2,3] ($1\cdot10^{-16}$-$6\cdot10^{-13}$[1,2,3])
	Brøggertinden	CP-35	360	sandstone, conglomerates	0.02-0.10[3]	$3\cdot10^{-17}$-$6\cdot10^{-13}$[2]
Precambrian	Nielsenfjellet		2500	Phyllite, quartzite		

[1]=Brown et. al., 1977,[2]=Domenico and Schwartz, 1990,[3]=Primary porosity and permeability measured on bedrock cores from Ny-Ålesund at Statoil's laboratorium, Trondheim,[4]=Dallman et. al., 1999.
The values between the brackets are estimated values for a non-karstified situation.

Annex D Field measurements

D.1 Discharge measurements

In this section the methods for measuring discharge will be explained. In section D.2 the results of the measurements are illustrated in figures. D.3 lists the measurement data.

D.1.1 Salt dilution method

A method for measurement of water discharge in turbulent streams is the relative salt dilution method. A volume of salt solution is injected suddenly into the stream, and the dilution is measured by means of the electrical conductivity (Hongve, 1987).
This method is used because it is a convenient method to measure discharge.
One kilo of salt (NaCl) was dissolved in a bucket of water and injected in the stream. Downstream the electrical conductivity was measured.
The recorded change in conductivity can be used directly for calculation of discharge. In the calculation it was not necessary to consider a temperature correction factor, since the electrical conductivity meter already accounts that.
Therefore the discharge can be calculated from:

$$Q = \frac{m \cdot 10^6 \cdot \gamma_{g,25}}{\int_0^t \Delta\gamma_\theta dt} \qquad \text{(D-1)}$$

With:
Q : discharge rate (l/s)
m : mass of salt (kg)
$\gamma_{g,25}$: conductivity of NaCl at the ambient electrical conductivity of the river water (at half top height) (mS/cm)
$\int_0^t \Delta\gamma_\theta dt$: the integral of the conductivity curve above the baseline as a function of time

$$\gamma_{g,25} = 0.214 - 0.0003\gamma_{25} \qquad \text{(D-2)}$$

With:
γ_{25} : conductivity of the river water (mS/cm)

A simple way of integration of $\int_0^t \Delta\gamma_\theta dt$ is to regard the curve as a time-step function.

$$\int_0^t \Delta\gamma_\theta dt \cong \sum_{i=1}^{i=n} t_{si} \cdot \gamma_{\theta i} - t_t \cdot \gamma_{25} \qquad \text{(D-3)}$$

With:
t_{si} : the sampling interval (s), i = 1,2,3

γ_a : the conductivity from the individual measurements, i = 1,2,3
t_t : total time of measurement (s)

D.1.2 Velocity area method

With the velocity area method the discharge is determined by measuring the flow velocities with a current meter.
A propeller type current meter was used.

The discharge is calculated from the velocity and depth measurements. This can be done according to different methods (Shaw, 1994).
With the mean section method, averages of the mean velocity in the verticals and of the depths at the boundaries of a section sub-division are taken and multiplied by the width of the sub-division:

$$Q = \sum q_i = \sum \bar{v} \cdot a = \sum_{i=1}^{n} \frac{(\bar{v}_{i-1} + \bar{v}_i)}{2} \frac{(d_{i-1} + d_i)}{2} (b_i - b_{i-1})$$

With:
$\bar{v}$: velocity [m/s]
a : area [m^2]
d_i : depth at sub-section i [m]
b_i : distance of the measuring point (i) from a bank datum
n : number of sub-sections [-]

With the mid section method, the mean velocity and depth measured at a sub-division point are multiplied by the segment width measured between the mid-points of neighbouring systems:

$$Q = \sum q_i = \sum \bar{v} \cdot a = \sum_{i=1}^{n} \bar{v}_i \cdot d_i \frac{(b_{i+1} - b_{i-1})}{2}$$

With:
n : the number of measured verticals and sub-areas

D.2 Results

In figure A4.1 the conductivity during the measurement is shown.
Figure A4.2 shows the depth and velocity, perpendicular to the flow direction.

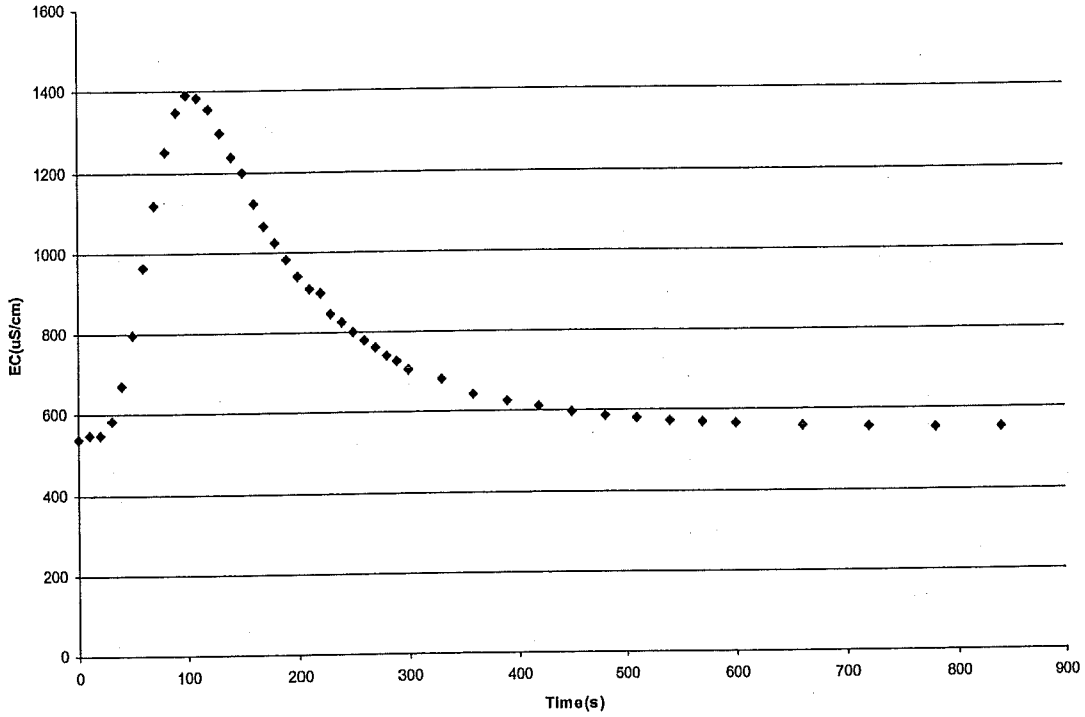

Figure D.1. Measured conductivity in time.

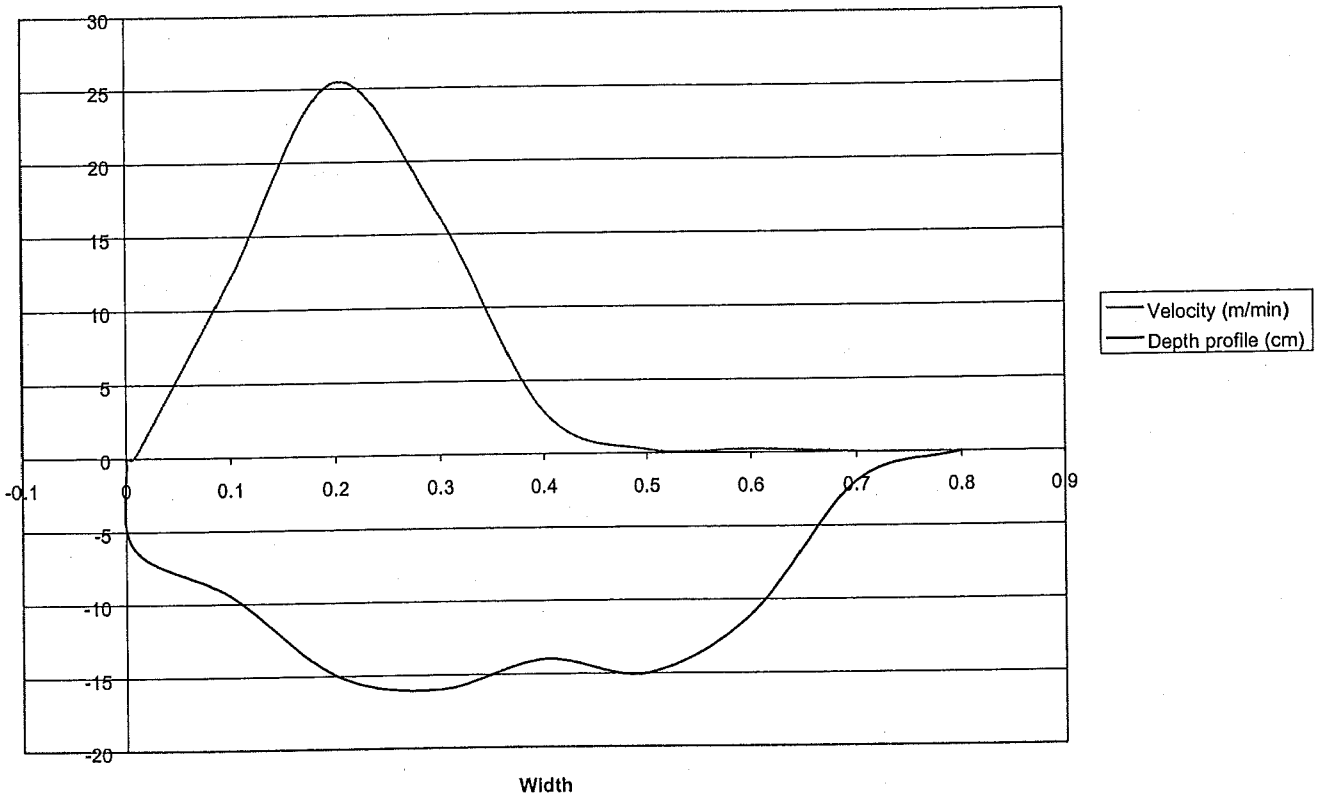

Figure D.2. Measured depth and velocity.

D.3 Measurements

Table D.1. Electrical conductivity (EC) during the salt dilution measurement.

Time (s)	*EC(μS/cm)*	*Time (s)*	*EC(μS/cm)*
0	537	450	598
10	550	460	
20	550	470	
30	583	480	588
40	670	490	
50	797	500	
60	964	510	580
70	1119	520	
80	1251	530	
90	1349	540	573
100	1391	550	
110	1382	560	
120	1354	570	570
130	1297	580	
140	1235	590	
150	1197	600	565
160	1122	610	
170	1066	620	
180	1025	630	
190	980	640	
200	941	650	
210	909	660	560
220	897	670	
230	846	680	
240	823	690	
250	799	700	
260	780	710	
270	762	720	555
280	742	730	
290	727	740	
300	704	750	
310		760	
320		770	
330	680	780	553
340		790	
350		800	
360	642	810	
370		820	
380		830	
390	627	840	551
400			
410			
420	611		
430			
440			

Table D.2. Velocity during the velocity area method.

b(m)	*d(m)*	*n(rotations/min)*	*v(m/min)*
0	0	0	0
0.1	0.062	0	0
0.2	0.095	118	12.061
0.3	0.15	249	25.423
0.4	0.16	159	16.243
0.5	0.14	28	2.881
0.6	0.15	2	0.229
0.7	0.11	2	0.229
0.8	0.02	0	0
0.9	0	0	0

Annex E Input Files

E.1 USEFIL File

USEFIL
MESH INPUT : mesh.in
MESH PRINT : meshprn
MESH : mesh.1
METROPOL LOG : mlog
METROPOL-3 INPUT : m3.in
METROPOL-3 SOURCE : m3src
METROPOL-3 PRINT : m3prn
METROPOL-3 TIME PROFILE : m3prof
METROPOL-3 RESTART INPUT : m3rin
METROPOL-3 RESTART OUTPUT : m3rout
METROPOL-3 UNFORMATTED OUTPUT : m3unf
METROPLOT INPUT : mplt.in
METROPLOT PRINT : mpltprn
METROPART INPUT : mpart.in
METROPART PRINT : mpartprn

E.2 Input file for METROHEAT

METROPOL-3 INPUT
MESH ID: 100
PROJECT: vestre Lovenbreen
1e opzet met x=2900m y=3000m en -500<z<350
elementen van 100*100 in xy, 100*50 in xz
END HEADING
0
001
51 15000 1e-10 1e-15
151 15000 1e-10 1e-15
151 15000 1e-10 1e-15
1 1e-2 1e-5 1e-5 1e-5 1e-5 20 3.2e9 864000
9.81 0 0 0
998.2 0.69 0.0 1e5 0.0 20
1 1.004e-3
0 0
0.6 4182.0
DISTRIBUTED DATA
startc.in
startt.in
cmat.in
densm.in
kx.in
kx.in
kx.in

tcondx.in
tcondx.in
tcondx.in
por.in
compr.in
long.in
trans.in
long.in
trans.in
diff.in
tensor.in
tensor.in
tensor.in
tensor.in
tensor.in
tensor.in
tensor.in
tensor.in
tensor.in
tensor.in
tensor.in
tensor.in
tensor.in
tensor.in
tensor.in
tensor.in
tensor.in
tensor.in
BOUNDARY CONDITIONS
SURFACE 1
22
1 639 22 8
-6.4
2 640 22 8
-5.1
3 641 22 8
-3.8
4 642 22 8
-2.5
5 643 22 8
-1.2
6 644 22 8
0.1
7 645 22 8
1.4
8 646 22 8
2.7
9 647 22 8
4.0

10 648 22 8
5.3
11 649 22 8
6.6
12 650 22 8
7.8
13 651 22 8
9.1
14 652 22 8
10.4
15 653 22 8
11.7
16 654 22 8
13.0
17 655 22 8
14.3
18 656 22 8
15.6
19 657 22 8
16.9
20 658 22 8
18.2
21 659 22 8
19.5
22 660 22 8
20.8
SURFACE 2
17
1 22 1 1
661 682 1 1
1321 1342 1 1
1981 2002 1 1
2641 2662 1 1
3301 3322 1 1
3961 3982 1 1
4621 4642 1 1
5281 5302 1 1
5941 5962 1 1
6601 6622 1 1
7261 7282 1 1
7921 7942 1 1
8581 8602 1 1
9241 9262 1 1
9901 9922 1 1
10561 10582 1 1
SURFACE 3
17
22 660 22 8
20.8

682 1320 22 8
19.05
1342 1980 22 8
17.3
2002 2640 22 8
15.55
2662 3300 22 8
13.8
3322 3960 22 8
12.05
3982 4620 22 8
10.3
4642 5280 22 8
8.55
5302 5940 22 8
6.8
5962 6600 22 8
5.05
6622 7260 22 8
3.3
7282 7920 22 8
1.55
7942 8580 22 8
-0.2
8602 9240 22 8
-1.95
9262 9900 22 8
-3.7
9922 10560 22 8
-5.45
10582 11220 22 8
-7.2
SURFACE 4
17
639 660 1 1
1299 1320 1 1
1959 1980 1 1
2619 2640 1 1
3279 3300 1 1
3939 3960 1 1
4599 4620 1 1
5259 5280 1 1
5919 5940 1 1
6579 6600 1 1
7239 7260 1 1
7899 7920 1 1
8559 8580 1 1
9219 9240 1 1
9879 9900 1 1

10539 10560 1 1
11199 11220 1 1
SURFACE 5
19
1 639 22 8
-6.4
661 1299 22 8
-6.45
1321 1959 22 8
-6.5
1981 2619 22 8
-6.55
2641 3279 22 8
-6.6
3301 3587 22 8
-6.65
3609 3609 1 2
2.6e6 0.0 0.0
3631 3939 22 8
-6.65
3961 4599 22 8
-6.7
4621 5259 22 8
-6.75
5281 5919 22 8
-6.8
5941 6579 22 8
-6.85
6601 7239 22 8
-6.9
7261 7899 22 8
-6.95
7921 8559 22 8
-7.0
8581 9219 22 8
-7.05
9241 9879 22 8
-7.1
9901 10539 22 8
-7.15
10561 11199 22 8
-7.2
SURFACE 6
21
10561 10879 1 8
-7.2
10880 10880 1 4
-2.85e-7 0.0 0.0
10881 10901 1 8

-7.2
10902 10902 1 4
-2.85e-7 0.0 0.0
10903 10923 1 8
-7.2
10924 10924 1 4
-2.85e-7 0.0 0.0
10925 10945 1 8
-7.2
10946 10946 1 4
-2.85e-7 0.0 0.0
10947 10967 1 8
-7.2
10968 10968 1 4
-2.85e-7 0.0 0.0
10969 10989 1 8
-7.2
10990 10990 1 4
-2.85e-7 0.0 0.0
10991 11011 1 8
-7.2
11012 11012 1 4
-2.85e-7 0.0 0.0
11013 11033 1 8
-7.2
11034 11034 1 4
-2.85e-7 0.0 0.0
11035 11055 1 8
-7.2
11056 11056 1 4
-2.85e-7 0.0 0.0
11057 11077 1 8
-7.2
11078 11078 1 4
-2.85e-7 0.0 0.0
11079 11220 1 8
-7.2
OVERWRITE
2
3888 2.7814706e6 0.0 0.0
3911 2.7814706e6 0.0 0.0
INTERNAL PRESSURE
0
INTERNAL SALT MASS FRACTION
0
INTERNAL TEMPERATURE
0
PROFILE POINTS
0 0 0

ELEMENTS FOR SUBROSION
0 0 0
OUTPUT TIMES
5
864000
0 1 1 1 0 1
3.2e7
0 1 1 1 0 1
3.2e8
0 1 1 1 0 1
3.2e9
0 1 1 1 0 1
3.2e10
0 1 1 1 0 1

E.3 Input file for MMESH

METROMESH INPUT
MESH ID: 100
PROJECT: vestre Lovenbreen
1e opzet met x=2900m, y= 3000m en -500<z<350
elementen van 100x100 in xy, 100x50 in xz
END HEADING
NUMBER OF POINTS
23 31 18
CORNERS
0.0 0.0 35.0
2200.0 0.0 -500.0
2200.0 3000.0 -500.0
0.0 3000.0 35.0
2000.0 0.0 350.0
2900.0 0.0 350.0
2900.0 3000.0 350.0
2000.0 3000.0 350.0
EDGE 1
1
EDGE 2
1
EDGE 3
1
EDGE 4
1
EDGE 5
1
EDGE 6
1
EDGE 7
1
EDGE 8

1
EDGE 9
1
EDGE 10
1
EDGE 11
1
EDGE 12
1
SURF 1
1
SURF 2
1
SURF 3
1
SURF 4
1
SURF 5
1
SURF 6
1
VOLUME
1
OUTPUT OPTIONS
1 1 0 0 0 0

E.4 RDARR file for permeability values

BEGIN RDARR
permeability (m^2)
2
1474
2640 1.0E-10
2654 1.0E-16
2656 1.0E-15
2660 2.0E-9
2662 1.0E-14
2676 1.0E-16
2678 1.0E-15
2682 2.0E-9
2684 1.0E-14
2698 1.0E-16
2700 1.0E-15
2704 2.0E-9
2706 1.0E-14
2720 1.0E-16
2722 1.0E-15
2726 2.0E-9
2728 1.0E-14

```
2742    1.0E-16
2744    1.0E-15
2748    2.0E-9
2750    1.0E-14
2764    1.0E-16
2766    1.0E-15
...
...
END RDARR
```

Annex F M-files

F.1 M-file for area plot of pressure data

```
load pressure.dat
x=pressure(:,1);
y=pressure(:,2);
z=pressure(:,3);
p=pressure(:,4);

sizex = length(x);
sizey = length(y);
for i=1:((sizex/23)-1)
    for j=1:23
        X(i,j)=x(23*i+j);
        Y(i,j)=y(23*i+j);
        Z(i,j)=z(23*i+j);
        P(i,j)=p(23*i+j);
    end
end

surf(X,Y,Z,P)
shading interp
H = colorbar('horiz');
xlabel('x (m)');
ylabel('y (m)');
zlabel('z (m)');
axis equal
```

F.2 M-file for surface plot of temperature data on y=1500m

```
load temperature.dat
tempnieuw(1:23,:) = temperature(346:368,:);
tempnieuw(24:46,:) = temperature(1059:1081,:);
tempnieuw(47:69,:) = temperature(1772:1794,:);
tempnieuw(70:92,:) = temperature(2485:2507,:);
tempnieuw(93:115,:) = temperature(3198:3220,:);
tempnieuw(116:138,:) = temperature(3911:3933,:);
tempnieuw(139:161,:) = temperature(4624:4646,:);
tempnieuw(162:184,:) = temperature(5337:5359,:);
tempnieuw(185:207,:) = temperature(6050:6072,:);
tempnieuw(208:230,:) = temperature(6763:6785,:);
tempnieuw(231:253,:) = temperature(7476:7498,:);
tempnieuw(254:276,:) = temperature(8189:8211,:);
tempnieuw(277:299,:) = temperature(8902:8924,:);
tempnieuw(300:322,:) = temperature(9615:9637,:);
tempnieuw(323:345,:) = temperature(10328:10350,:);
tempnieuw(346:368,:) = temperature(11041:11063,:);
tempnieuw(369:391,:) = temperature(11754:11776,:);
```

```
tempnieuw(392:414,:) = temperature(12467:12489,:);

x = tempnieuw(:,1);
y = tempnieuw(:,2);
z = tempnieuw(:,3);
t = tempnieuw(:,4);

sizex = length(x);
sizey = length(y);
for i=1:((sizex/23)-1)
    for j=1:23
        X(i,j)=x(23*i+j);
        Y(i,j)=y(23*i+j);
        Z(i,j)=z(23*i+j);
        T(i,j)=t(23*i+j);
    end
end

v = [0 0];
contour(X,Z,T,v,'w');
hold on;
pcolor(X,Z,T)
shading interp
hold off;

H = colorbar('horiz');
xlabel('x (m)');
ylabel('z (m)');
axis equal
axis tight

figure(2)
surf(X,Y,Z,T)
shading interp
hold on;
load raam.dat
X=raam(:,1);
Y=raam(:,2);
Z=raam(:,3);
plot3(X,Y,Z)
hold off;
I = colorbar('horiz');
xlabel('x (m)');
ylabel('y (m)');
zlabel('z (m)');
```

F.3 M-file for surface plot of log avaraged effective velocity

```
load velocity.dat
```

```
velonieuw(1:22,:) = velocity(331:352,:);
velonieuw(23:44,:) = velocity(991:1012,:);
velonieuw(45:66,:) = velocity(1651:1672,:);
velonieuw(67:88,:) = velocity(2311:2332,:);
velonieuw(89:110,:) = velocity(2971:2992,:);
velonieuw(111:132,:) = velocity(3631:3652,:);
velonieuw(133:154,:) = velocity(4291:4312,:);
velonieuw(155:176,:) = velocity(4951:4972,:);
velonieuw(177:198,:) = velocity(5611:5632,:);
velonieuw(199:220,:) = velocity(6271:6292,:);
velonieuw(221:242,:) = velocity(6931:6952,:);
velonieuw(243:264,:) = velocity(7591:7612,:);
velonieuw(265:286,:) = velocity(8251:8272,:);
velonieuw(287:308,:) = velocity(8911:8932,:);
velonieuw(309:330,:) = velocity(9571:9592,:);
velonieuw(331:352,:) = velocity(10231:10252,:);
velonieuw(353:374,:) = velocity(10891:10912,:);

x = velonieuw(:,1);
y = velonieuw(:,2);
z = velonieuw(:,3);
vlog = velonieuw(:,8);

sizex = length(x);
sizey = length(y);
for i=1:((sizex/22)-1)
    for j=1:22
        X(i,j)=x(22*i+j);
        Y(i,j)=y(22*i+j);
        Z(i,j)=z(22*i+j);
        Vlog(i,j)=vlog(22*i+j);
    end
end

contour(X,Z,Vlog,0);
hold on;
pcolor(X,Z,Vlog)
shading interp
H = colorbar('horiz');
xlabel('x (m)');
ylabel('z (m)');
hold off;
axis equal
axis tight
```

F.4 M-file for 3-D mesh plot (Figure 4.3)

```
load temperature.dat
x=temperature(:,1);
```

```
y=temperature(:,2);
z=temperature(:,3);
t=temperature(:,4);

sizex=length(x);sizey=length(y);
for i=1:((sizex/23)-1)
    for j=1:23
        X(i,j)=x(23*i+j);
        Y(i,j)=y(23*i+j);
        Z(i,j)=z(23*i+j);
        T(i,j)=t(23*i+j);
    end
end

mesh(X,Y,Z,T);
colormap([0 0 0]);
```